Olfactory ensheathing cells from adult female rats are hybrid glia that promote neural repair

Patricia E. Phelps*, Sung Min Ha, Rana R. Khankan, Mahlet A. Mekonnen, Giovanni Juarez, Kaitlin L. Ingraham Dixie, Yen-Wei Chen and Xia Yang*

Department of Integrative Biology and Physiology
UCLA, Los Angeles, CA 90095

*Corresponding author:
Patricia E. Phelps, Ph.D.
UCLA, Dept. of Integrative Biology and Physiology
Terasaki Life Sciences Building
610 Charles Young Dr. East
Los Angeles, CA 90095-7239
Telephone: (310) 825-7264
Email: pphelps@physci.ucla.edu

*Corresponding author:
Xia Yang, PhD.
UCLA, Dept. of Integrative Biology and Physiology
Terasaki Life Sciences Building
610 Charles Young Dr. East
Los Angeles, CA 90095-7239
Email: xyang123@ucla.edu

Abbreviated title: OECs are hybrid glia
Number of pages: 52
Number of figures: 9
Number of Supplemental figures: 3
Number of Supplemental tables: 4
Key words: scRNA-seq, OECs, Reelin (*Reln*), Connective tissue growth factor (*Ctgf/Ccn2*), neural repair

Acknowledgments: This work was supported by the National Institute of Neurological Disorders and Stroke: RO1 NS076976 (PEP), R01 NS111378 (XY), R01 NS117148 (XY), and by NICHD of the National Institutes of Health under award number P50HD103557. Additional support came from the UCLA QCBio Collaboratory Postdoc Fellowship (SMH), Eureka fellowship (RRK), MARC U*STAR fellowship T34 GM008563 (GJ), and UCLA Graduate Year Fellowship (KLID). We thank Drs. Julie Miller and Stephanie White for their generosity and considerable assistance with western blots, Drs. Hui Zhong and VR Edgerton for their long-term collaboration on spinal cord injury studies, and Sun Young Lee for excellent technical assistance.

Data availability: Raw scRNA-seq data and expression matrix is available at GEO (accession number GSE215247). The scRNA-seq results also can be viewed interactively at the Single Cell Portal. OEC vs Leftovers: https://singlecell.broadinstitute.org/single_cell/study/SCP1237/leftovers-and-oecs. OEC subclusters:https://singlecell.broadinstitute.org/single_cell/study/SCP1489/oec-subcluster-batch-corrected

Conflict of Interest: The authors declare no competing interests.

Abstract

Olfactory ensheathing cells (OECs) are unique glial cells found in both central and peripheral nervous systems where they support continuous axonal outgrowth of olfactory sensory neurons to their targets. Previously we reported that following severe spinal cord injury, OECs transplanted near the injury site modify the inhibitory glial scar and facilitate axon regeneration past the scar border and into the lesion. To better understand the mechanisms underlying the reparative properties of OECs, we used single-cell RNA-sequencing of OECs from adult rats to study their gene expression programs. Our analyses revealed five diverse OEC subtypes, each expressing novel marker genes and pathways indicative of progenitor, axonal regeneration, secreted molecules, or microglia-like functions. We found substantial overlap of OEC genes with those of Schwann cells, but also with microglia, astrocytes, and oligodendrocytes. We confirmed established markers on cultured OECs, and localized select top genes of OEC subtypes in olfactory bulb tissue. We also show that OECs secrete Reelin and Connective tissue growth factor, extracellular matrix molecules which are important for neural repair and axonal outgrowth. Our results support that OECs are a unique hybrid glia, some with progenitor characteristics, and that their gene expression patterns indicate functions related to wound healing, injury repair and axonal regeneration.

Introduction

Olfactory sensory neurons (OSNs) are remarkable as they undergo life-long neurogenesis within the adult olfactory epithelium (Graziadei & Monti Graziadei, 1985), and their axons are exclusively associated with a specialized type of glia, olfactory ensheathing cells (OECs; Doucette, 1990). OECs provide the outgrowth and guidance factors needed for OSN axons to reach their glomerular targets and exhibit regenerative abilities in response to injury (Doucette, 1991; Li et al., 2005; Williams et al., 2004). OECs have received considerable interest due to their ability to support axonal outgrowth even after severe or complete spinal cord transection in rodents, dogs and humans (Granger et al., 2012; Khankan et al., 2016; Ramon-Cueto et al., 2000; Tabakow et al., 2014; Takeoka et al., 2011; Thornton et al., 2018).

The regenerative capacity of adult spinal cord neurons is inhibited by the lesion site environment that includes a reactive glial scar, together with invading meningeal fibroblasts and multiple immune cells (Burda & Sofroniew, 2014; Wanner et al., 2013). The lesion core is composed of non-neural tissue that inhibits axonal outgrowth due to the upregulation and secretion of chondroitin sulfate proteoglycans that impede axon regeneration (Cregg et al., 2014). Some studies of severe or complete spinal cord transection in rats followed by the transplantation of OECs provided evidence that OECs surround axon bundles which regenerate into and occasionally across the injury site (Khankan et al., 2016; Ramon-Cueto et al., 2000; Takeoka et al., 2011; Thornton et al., 2018). In combination with *in vitro* studies, detailed analyses of injury sites suggest that OECs: 1) function as phagocytes to clear degenerating axonal debris and necrotic cells (Khankan et al., 2016; Nazareth et al., 2020; Su et al., 2013), 2) modulate the immune response to injury (Khankan et al., 2016; Vincent et al., 2007), and 3) interact favorably with the glial scar and lesion core that form after injury *in vitro*, (Lakatos et

al., 2003; Lakatos et al., 2000) and *in vivo*, (Khankan et al., 2016; Thornton et al., 2018). OEC transplantation following complete spinal cord transection creates an environment that is conducive to neural repair (Khankan et al., 2016; Takeoka et al., 2011; Thornton et al., 2018). OECs secrete molecules that stimulate axon outgrowth such as Brain-derived neurotrophic factor (Bdnf), Nerve growth factor (Ngf), and Laminin (Ruitenberg et al., 2003; Runyan & Phelps, 2009; Woodhall et al., 2001) and enhance cell-to-cell mediated interactions between neurites and OECs in an inhibitory environment (Chung et al., 2004; Khankan et al., 2015; Windus et al., 2007). Khankan et al. (2015) showed that neurites grew 2-3 times longer in growth-inhibitory areas of multicellular 'scar-like' cultures when they were directly associated with olfactory bulb-derived OECs (OB-OECs), but the molecular mechanisms are unknown.

The outcomes of OEC transplantation studies after spinal cord injury vary substantially in the literature due to many technical differences in their experimental designs. The source of OECs has a great impact on the outcome, with OB-OECs showing more promise than lamina propria-derived OECs, and purified, freshly-prepared OECs being required for optimal OEC survival. Other important variables include the severity of the injury (hemisection to complete spinal cord transection), the age of the spinal cord injured host (early postnatal versus adult), and OEC transplant strategies (delayed or acute transplantation, cell transplants with or without a matrix; Franssen et al., 2007). Franssen et al. (2007) evaluated OEC transplantation studies, and reported that 41 out of 56 studies showed positive effects, such as stimulation of regeneration, positive interactions with the glial scar and remyelination of axons. More recent reviews and meta-analyses of the effects of OEC transplantation following different spinal cord injury models reported that OECs significantly improved locomotor function (Watzlawick et al., 2016; Nakjavan-Shahraki et al., 2018).

Together with collaborators, we conducted six spinal cord injury studies in adult rats with a completely transected, thoracic spinal cord model followed by OB-OEC transplantation (Kubasak et al., 2008; Takeoka et al., 2011; Ziegler et al., 2011; Khankan et al., 2016; Thornton et al., 2018; Dixie, 2019). Results from five of the six studies showed physiological and/or anatomical evidence of axonal regeneration into and occasionally across the injury site. In 6-8-month-long studies, Takeoka et al. (2011) and Ziegler et al. (2011) reported physiological evidence of motor connectivity across the transection in OEC- but not media-transplanted rats. These experiments used transcranial electric stimulation of the motor cortex or brainstem to detect motor-evoked potentials (MEPs) with EMG electrodes in hindlimb muscles at 4- and 7-months post-transection. After 7 months, 70% of OEC-treated rats responded to stimulation with hindlimb MEPs (motor cortex, 5/20; brainstem 12/20; Takeoka et al, 2011). A complete re-transection above the original transection was carried out one month later and all MEPs in OEC-injected rats were eliminated. These results provide physiological evidence of axon conductivity across the injury site in OEC-treated rats. Additionally, three of our long-term studies evaluated anatomical axonal outgrowth of the descending serotonergic Raphespinal pathway into and through the injury site. Significantly more serotonergic-labeled axons crossed the rostral inhibitory scar border (Takeoka et al., 2011) or occupied a larger area within the injury site core (Thornton et al., 2018, Dixie, 2019) in OEC-transplanted rats than in fibroblast or media controls. In addition, significantly more neurofilament-labeled axons were found within the lesion core of OEC-transplanted versus control rats (Thornton et al., 2018, Dixie, 2019).

The question addressed in the present study is how OB-OECs perform the diverse functions associated with neural repair. We hypothesize that there exist OB-OEC subtypes, and that their respective gene programs and secreted molecules underlie their multifaceted reparative

activities. Here we identify the OB-OEC subtypes and their molecular programs that contribute to injury repair, such as the growth-stimulating secreted and cell adhesion molecules involved in OB-OEC interactions that promote neurite and axonal outgrowth. We used single-cell RNA-sequencing (scRNA-seq) to characterize the immunopurified female rat OB-OECs (hereafter called OECs unless stated otherwise) that are similar to those transplanted into our previous female rat spinal cord injury studies. We first compared the genes expressed by purified OECs with those expressed by the 'leftover cells', i.e., the cells which are not selected by the panning procedure, to determine if the purification process selected for specific OEC subtypes. After confirming the characteristic OEC markers, our scRNA-seq data revealed five OEC subtypes which expressed unique marker genes and were further characterized and confirmed experimentally. Finally, we examined interesting extracellular matrix (ECM) molecules secreted by OECs, Reelin (*Reln*) and Connective tissue growth factor (*Ccn2*/*Ctgf*), both of which may facilitate axonal outgrowth into the inhibitory injury core environment.

Results

One particularly challenging aspect facing neural repair of spinal cord injury (SCI) is to facilitate axonal outgrowth and eventually regeneration across the inhibitory injury site. A common finding in our studies testing the effects of OEC transplantation following SCI is that OECs modify the injury site so that some axons project past the glial scar and into the lesion core surrounded by OECs (Dixie, 2019; Khankan et al., 2016; Takeoka et al., 2011; Thornton et al., 2018). Figure 1 shows an enlargement of an injury site which contains green fluorescent protein (GFP)-labeled OECs in the glial fibrillary acidic protein (GFAP)-negative injury core between the two GFAP-positive spinal cord stumps. The OECs in the injury core are associated with a

few serotonergic- (Figure 1a-f) and many neurofilament-labeled axons (Figure 1g-l). We note, however, that such bridge formation is rare following severe spinal cord injury in adult mammals and was detected in 2 out of 8 OEC-transplanted rats versus 0/11 media or fibroblast-transplanted controls in this study (Dixie, 2019). Combined with the 1/5 OEC-transplanted rats with axons crossing the injury and 0/5 fibroblast controls in our previous study (Thornton, 2018), we observed bridges in 3/13 OEC-transplanted rats vs 0/16 controls (p=0.042, two-sample proportion test). Bridge formation, in conjunction with the additional physiological and anatomical evidence of axonal connections across the injury site presented in our previous studies, strongly supports the capacity of OECs in neural repair. To learn more about possible mechanisms by which OECs support axon regeneration, we prepared immunopurified OECs and examined their gene expression and diversity with scRNA-seq.

Unbiased scRNA-seq of immunopurified OECs and 'leftover' controls distinguishes OECs, microglia, and fibroblasts.

Using scRNA-seq, we sequenced a total of 65,481 cells across 7 samples (n=3 OEC preparations and 4 'leftover' controls) that passed quality control, with an average of 9,354 cells per sample. Cell clusters were visualized using t-distributed stochastic neighbor embedding (tSNE). The tSNE plot showed that cells from immunopanned OEC samples were separated from the cells from the leftover samples (Figure 2a). Cell clustering analysis defined a total of seven clusters (Figure 2b), each of which showed expression patterns of marker genes that distinguish one cluster from the others (Figure 2c). Based on previously reported cell type marker genes for fibroblasts and major glial cell types including OECs, astrocytes, oligodendrocytes, and microglia, we found elevated expression of OEC marker genes in clusters 2, 3 and 7, microglia

marker genes in clusters 4, 6, and 7, and fibroblast marker genes in clusters 0, 1, and 5 (Figure 2d, Suppl. Figure 1). In contrast, except a few select genes, the majority of markers for astrocytes and oligodendrocytes showed low expression (Figure 2d). The cell cluster tSNE plot with cell type labels in Figure 2e, and the distinct expression patterns of cell type markers are confirmed in a dot plot in Figure 2f. As expected, many cells enriched in the leftover controls were defined as fibroblasts and microglia based on the corresponding known marker genes, whereas cells from the immunopanned OEC samples showed high expression of OEC marker genes (Figure 2a vs. 2e). After cell type assignment, a dot plot clearly depicts distinct expression of cell type-specific marker genes (Figure 2f). Our scRNA-seq results support the expected cell type composition following the immunopanning procedure. All marker genes for each major cell type, including statistics, are in Suppl. Table 1.

We next asked if there were differences between cultures of immunopurified OECs and OECs grown in 'leftover' cultures. While our previous spinal cord injury studies transplanted 90-95% purified OECs, other labs culture and implant less purified OECs and thus many of the neighboring cells, i.e., primarily fibroblasts and microglia, would be included. Our comparison showed that purified OECs express higher levels of *Cryab* (stress protection, inflammation inhibition), *Nqo1* (antioxidant protection, stress adaptation), and *Postn* (cell proliferation, survival, migration) genes (Figure 2g), whereas OECs in leftover cultures with fibroblasts and microglia express higher levels of *Apoe* (lipid transport and glial function), *Calcb* (inflammation and pain modulation), and *Mgp* (ECM calcium inhibitor; Figure 2g) than purified OECs. These results indicate immunopurified OECs may have better stress response and proliferative and survival capacity than the controls.

Immunofluorescence verification of typical OEC marker genes revealed by scRNA-seq

To validate the OEC markers revealed by scRNA-seq, we re-cultured extra cells not used for sequencing for immunocytochemical confirmation. Because our adult OECs are immunopurified with anti-nerve growth factor receptor p75 ($Ngfr^{p75}$), we expected and found OEC samples heavily enriched in $Ngfr^{p75}$ in both immunofluorescence (Figure 3a) and scRNA-seq (Figure 3b). Next, we detected the high expression of two common glial markers, Blbp (*Fabp7;* Figure 3c, 3d) and S100β (Figure 3e, 3f), in OECs. Sox10 is expressed in the nuclei of neural crest-derived cells such as OECs and Schwann cells, and our cultures showed high expression levels in scRNA-seq and immunocytochemistry (Figure 3c, 3g, 3k, 3m). Three cell adhesion molecules, L1-Cam (Figure 3g, 3h; Runyan & Phelps, 2009; Witheford et al., 2013), N-Cam (Figure 3i, 3j), and N-Cadherins (Figure 3k, 3l), are also expressed in purified OEC cultures. In addition, other previously reported OEC genes are now verified by scRNA-seq, including the pro-myelinating Ciliary neurotrophic factor (*Cntf*, Figure 3n; Asan et al., 2003; Roet et al., 2011), the laminin receptor α7 integrin (*Itga* 7, Figure 3o; Ingram et al., 2016), and the myelin related gene P0 (*Mpz*, Figure 3p; Sasaki et al., 2006). Thus, well-characterized OEC markers were detected by scRNA-seq and most are widely distributed among OEC clusters.

In addition to confirming select genes, we also compared the 209 significant OEC markers identified from our scRNA-seq data with the 309 genes from the meta-analysis of five OEC microarray studies on cultured early-passage OB-OECs versus other tissues (Roet et al., 2011). We found 63 genes overlapping between our OEC markers and the published markers, representing a 15.3-fold overlap enrichment (p-value: 4.3 e-58), further supporting the reliability of our scRNA-seq findings.

Subclustering analysis of OECs revealed refined OEC subtypes and their top marker genes. Next, we extracted OECs and performed a subclustering analysis with OECs alone, and found five distinct subclusters (Figure 4a). All subclusters except for cluster 3 expressed previously identified markers of OECs as well as subsets of marker genes for astrocytes, oligodendrocytes, and Schwann cells (Figures 4b, c). The percentage of OECs within each cluster that express a gene, the percentage of OECs in all other subtypes that express a gene and their p values are found in Suppl. Table 2. Interestingly, cluster 3 showed expression of both microglia and OEC markers. The top 20 genes expressed by each OEC subtype were investigated to evaluate potential functional differences between the subtypes (Figure 4c; Suppl. Table 3), and their enriched pathways (Figure 4d). Most references for the specific genes within the clusters are found in Suppl. Table 3.

Cluster 0 is rich in matricellular proteins. Pathway enrichment analysis showed that ECM organization and collagen biosynthesis were significantly enriched in the marker genes for the largest OEC subcluster 0 (Figure 4d). Two of the top 10 genes are members of the Ccn family of matricellular proteins, *Ccn2*/*Ctgf* (Connective tissue growth factor; Figure 5a) and *Ccn3/NOV* (nephroblastoma overexpressed gene; Figure 5b, Suppl. Table 3). Both are secreted ECM proteins which regulate the activity of growth factors and cytokines, function in wound healing, cell adhesion, and injury repair. The presence of *Ccn3* in OECs is novel, while *Ccn2/Ctgf* is well established (Lamond & Barnett, 2013; Roet et al., 2011). In figures 5c, c1-2, we show that *Ccn2* and *Sox10* are highly expressed in our cultured OECs. Because Mokalled et al. (2016) reported that *Ctgf*α is a critical factor required for spontaneous axon regeneration following spinal cord injury site in zebrafish, we asked if GFP-labeled OECs transplanted 2 weeks following a complete spinal cord transection in adult rats, also expressed Ccn2/Ctgf. We

found high levels of Ctgf expression in GFP-OECs (n=4 rats) that bridged much of the injury site and also detected Ctgf on near-by cells (Figure 5d, d1-2). GFP-labeled fibroblast transplantations (n=3 rats) served as controls and also expressed Ctgf. Other top ECM genes are *Serpinf1* (Serine protease inhibitor), *Fbln2* (Fibulin2), *Fn1* (Fibronectin-1), and *Col11a1* (Collagen, type XI, alpha 1; Suppl. Table 3).

The top-ranked marker gene for cluster 0 is *Pmp22* (Peripheral myelin protein 22), a tetraspan membrane glycoprotein that is highly expressed in myelinating Schwann cells, and contributes to the membrane organization of compact peripheral myelin. The third-ranked gene, *Gldn* (Gliomedin) is secreted by Schwann cells and contributes to the formation of the nodes of Ranvier. *Fst* (Follistatin) also plays a role in myelination and is expressed in areas of adult neurogenesis.

Many of the top cluster 0 genes are found in other glial cells: *Fbln2* is secreted by astrocytes, *Ccn2/Ctgf* is expressed by astrocytes and Schwann cells, *Nqo1* (NAD(P)H dehydrogenase, quinone 1 enzyme) is found in Bergmann glia, astrocytes, and oligodendrocytes, and *Marcks* (Myristoylated alanine-rich C-kinase substrate protein) regulates radial glial function and is found in astrocytes and oligodendrocytes. In addition, *Cd200* is expressed by astrocytes and oligodendrocytes, and binds to its receptor, *Cd200R*, on microglial cells. Thus, the OECs in cluster 0 express high levels of genes found in other glia, many of which are related to ECM and myelination.

Cluster 1 contains classic OEC markers. Three of the top five genes in cluster 1, *Pcsk1* (proprotein convertase PC1), *Gal* (neuropeptide and member of the corticotropin-releasing factor family) and *Ucn2* (Urocortin-2) were reported in the meta-analysis by Roet et al. (2011). Galanin

is expressed by neural progenitor cells, promotes neuronal differentiation in the subventricular zone and is involved in oligodendrocyte survival.

A well-known oligodendrocyte and Schwann gene associated with myelin, *Cnp* (2-3-cyclic nucleotide 3-phosphodiesterase), was high in OEC cluster 1 in addition to the cytokine *Il11* (Interleukin 11) that is secreted by astrocytes and enhances oligodendrocyte survival, maturation and myelin formation. The chondroitin sulfate proteoglycan Versican (*Vcan*) is another top gene expressed by astrocytes and oligodendrocyte progenitor cells.

Many of the genes and pathways that characterize cluster 1 are involved in nervous system development and axon regeneration (*Atf3, Btc, Gap43, Ngfr*^{p75}*, Bdnf, Pcsk1)*, and are found in other glia (Suppl. Table 3). Interestingly, after nerve injury, *Atf3* (cyclic AMP-dependent transcription factor 3) is upregulated by Schwann cells in the degenerating distal nerve stump and downregulated after axon regeneration is complete (Hunt et al., 2004). *Btc* (Betacellulin), part of the Epidermal growth factor (Egf) family and a ligand for Egfr, also is expressed by Schwann cells after nerve injury in a pattern similar to that of *Atf3*, as is Brain-derived neurotrophic factor (*Bdnf*). In addition, the proprotein convertase PC1 (*Pcsk1*) cleaves pro-Bdnf into its active form in Schwann cells and therefore also contributes to axon outgrowth. Together, the OECs in cluster 1 secrete a number of important growth factors associated with regeneration, including a novel one, *Atf3*, reported here (Suppl. Table 3).

Cluster 2 represents a distinctive proliferative OEC subtype. Most top genes in cluster 2 (Figure 6a-f) regulate the cell cycle (*Mki67, Stmn1, Cdk1, Cks2, Cdkn3, Cdca8, Cdca3*), are associated with mitosis (*Cenpf, Spc24, Tpx, Ckap2, Prc1, Ube2c, Top2a*), or contribute to DNA replication and repair (*Dut, Fam111a*, Suppl. Table 3). The top ranked gene, *Stmn1* (Stathmin 1; Figure 6e), is a microtubule destabilizing protein that is widely expressed in other OEC clusters

and in areas of adult neurogenesis. Pathway enrichment confirms the proliferative property of cluster 2 with pathways such as G1/S transition of mitotic cell cycle and DNA replication (Figure 4d). These results show that there are distinct OEC progenitors in our cultures within the olfactory nerve layer of the adult olfactory bulb.

MKi67 is a well-known proliferation gene concentrated in cluster 2 (Figure 6f). Previous studies suggested the presence of two morphologically distinct OECs – the Schwann-cell-like, spindle-shaped OECs with high $Ngfr^{p75}$ expression and the astrocyte-like, large flat OECs with low $Ngfr^{p75}$ (Franceschini & Barnett, 1996). To determine if the proliferative OECs differ in appearance from adult OECs, and whether there is concordance between our OEC subtypes based on gene expression markers and previously described morphology-based OEC subtyping (Franceschini & Barnett, 1996), we analyzed OECs identified with the anti-Ki67 nuclear marker and anti-$Ngfr^{p75}$(Figure 6g-h). Of the Ki67-positive OECs in our cultures, 24% ± 8% were strongly $Ngfr^{p75}$-positive and spindle-shaped, whereas 76% ± 8% were flat and weakly $Ngfr^{p75}$-labeled (n=4 cultures, p= 0.023). Here we show that a large percentage (~3/4^{ths}) of proliferative OECs are characterized by large, flat morphology and weak $Ngfr^{p75}$ expression resembling the previously described morphology-based astrocyte-like subtype. Our results indicate the two types of OEC classifications share certain degrees of overlap, indicating similarities but also differences between the two classification methods.

<u>*Cluster 3 resembles both microglia and OECs.*</u> In addition to the typical OEC markers (*$Ngfr^{p75}$*, *S100b*, and *Sox10*), cluster 3 also expressed numerous microglia markers (Figure 4b). In fact, all top 20 genes in cluster 3 are expressed in microglia, macrophages, and/or monocytes (Suppl. Table 3). Microglia markers in the top 20 genes include *Tyrobp,* which functions as an adaptor for a variety of immune receptors, *Cst3* (Cystatin C), *Anxa3* (Annexin A3), *Aif1 (*Iba-1),

and *Cd68*. OECs are known to endocytose bacteria and degrade axons, and therefore participate in the innate immune function (Khankan et al., 2016; Leung et al., 2008; Nazareth et al., 2015; Vincent et al., 2007). We also observed relatively high expression of genes involved in lysosome functions, such as *Cst3, Ctsz, Laptm5, Ctsb*, and *Lyz2*, compared to those in other OEC clusters (Figure 4e). Three additional top genes are involved in the complement system (*C1qA, C1qb,* and *C1qc)*, and cluster 3 pathways are highly enriched for inflammatory response and neutrophil immunity (Figure 4d).

Smithson and Kawaja (2010) identified unique microglial/macrophages that immunolabeled with Iba-1 (*Aif1*) and Annexin A3 (*Anxa3*) in the olfactory nerve and outer nerve layer of the olfactory bulb. These authors proposed that Iba1-Anxa3 double-labeled cells were a distinct population of microglia/macrophages that protected the olfactory system against viral invasion into the cranial cavity. Based on our scRNA-seq data we offer an alternative interpretation that at least some of these Iba-1-Anxa3 cells may be a hybrid OEC-microglial cell type. Supporting this interpretation, there are a number of reports that suggest OECs frequently function as phagocytes (e.g., Khankan et al., 2016; Nazareth et al., 2020; Su et al. 2013).

Cluster 4 has characteristics of astrocytes and oligodendrocytes. Cluster 4 is quite small. Its top two marker genes, *Sidt2*, a lysosomal membrane protein that digests macromolecules for reutilization and *Ckb*, a brain-type creatine kinase which fuels ATP-dependent cytoskeletal processes in CNS glia, are found in other OEC clusters. Four top genes, however, appear almost exclusively in cluster 4: 1) *Npvf* (Neuropeptide VF precursor/Gonadotropin-inhibitory hormone) inhibits gonadotropin secretion in several hypothalamic nuclei, and is expressed in the retina, 2) *Stmn2* (Stathmin2) is a tubulin-binding protein that regulates microtubule dynamics, 3) *Vgf* (non-acronymic) is synthesized by neurons and neuroendocrine cells and promotes

oligodendrogenesis, and 4) *Mt3* (Metallothionein-3) is a small zinc binding protein associated with growth inhibition and copper and zinc homeostasis (Suppl. Table 3).

Other genes expressed by cluster 4 are either expressed by other glia and/or are ECM molecules. Five genes are associated with both oligodendrocytes and astrocytes *(Ckb, C1ql1, Gria2, Stmn2, Ntrk2,* Suppl. Table 3). Among these, the astrocytic gene *C1ql1* is a member of the Complement component 1q family and regulates synaptic connectivity by strengthening existing synapses and tagging inactive synapses for elimination. Astrocytic Thrombospondin 2 (*Thbs2*) also controls synaptogenesis and growth. Other genes reported in astrocytes include *Ptn* (Pleiotrophin), *Igfbp3* (Insulin-like growth factor binding protein 3), and *Mt3,* whereas *Gpm6b* (Glycoprotein M6b) is involved in the formation of nodes of Ranvier in oligodendrocyte and Schwann cell myelin. Cluster 4 also has a significant enrichment for genes involved in ECM organization (Figure 4d; *Actn1, Col81a, Bgn, Fn1* and *Timp2*), together with clusters 0 and 1, as well as genes involved in positive regulation of cell migration together with cluster 3 (Figure 4f).

Trajectory and potential interactions among OEC subclusters

We performed pseudotime trajectory analysis using the Slingshot algorithm to infer lineage trajectories, cell plasticity and lineages by ordering cells in pseudotime based on their transcriptional progression reflected in our scRNA-seq data. Transcriptional progression refers to the changes in gene expression profiles of cells as they undergo differentiation or transition through different states. The trajectory analysis results suggest that there are potential transitions between specific OEC subclusters. Our results show that there are two distinct trajectories (Figure 4g). The first trajectory involves clusters 2, 0 and 4, whereas the second involves clusters 2, 0, 1, and 3. Although the directionality of these trajectories is indistinguishable, the fact that

cluster 2 is enriched for cell cycle genes and is the converging point of both trajectories, suggests that cluster 2 proliferates into the other OEC clusters. The predicted trajectories based on our scRNAseq data suggest plasticity in the cell clusters.

We also modeled potential autocrine/paracrine ligand-receptor interactions between OEC subclusters using NicheNet (Figure 4h). This analysis revealed that clusters 0, 1, and 2 have more ligands going to other OEC clusters, whereas clusters 3 and 4 generally receive ligands from other clusters. The network also showed that clusters 0, 1 and 4 express genes encoding neurotropic factors such as Bdnf, Cntf and Neurturin (*Ntrn*), that are involved in neuronal survival and neurite outgrowth. *Gal* from cluster 1 is a mediator for glia-glia, and glia-neuron communication (Gresle et al., 2015; Ubink et al., 2003). We found that cluster 4 secretes colony stimulating factor 1 (*Csf1*) which also shows potential regulation of cluster 3 through *Csf1r*. Overall, the trajectory and network analyses support potential cell plasticity and lineage relationships and cell-cell communications across OEC subclusters.

Spatial confirmation of defined OEC subclusters within the olfactory nerve layer *in situ*

Here we confirm, at the protein level, that some of the top genes derived from cultured OECs clusters are expressed in sections of the olfactory system from 8-10-week-old female Sprague Dawley rats. Our results illustrate the spatial distribution of 2-3 top genes from clusters 0 to 3 in the olfactory nerve layer (Figure 7; corresponding tSNE plots are in Suppl. Figure 2 for comparison). In cluster 0 we show high levels of Peripheral myelin protein 22 (Pmp22) in OECs (Figure 7a) with the remainder of the olfactory bulb unlabeled. The small protein Gliomedin (Gldn) is a component of Schwann cell microvilli and facilitates the formation of peripheral nodes of Ranvier (Eshed et al., 2005). Here we detect numerous small dot-like structures that

overlay the olfactory nerve layer (Figures 7b, c). The detection of high levels of Gldn in nonmyelinating OECs without nodes of Ranvier is surprising and suggests that it may also function as a glial ligand associated with olfactory sensory neuron axons. For cluster 1, we examined the expression of the important axonal growth factor Activating transcription factor 3 (Atf3*)* and confirmed that OECs express it widely (Figure 7d). Growth associated protein 43 (Gap43), a well-established marker of OECs and immature olfactory sensory neurons, is highly expressed in the olfactory nerve layer and at a lower level in the glomeruli of the olfactory bulb (Figure 7e). Nestin (Nes), an intermediate filament associated with neural stem cells, is widely expressed in the olfactory nerve layer (Figure 7f).

Compared to the two large clusters, the remaining clusters contain more specialized OECs. The top marker in the proliferative cluster 2 is Stathmin1 (Stmn1), encoding a microtubule destabilizing protein found in areas of adult neurogenesis (Boekhoorn et al., 2014). Stathmin 1 immunoreactivity (Figure 7g, Suppl. Figure 2) is detected in all OEC clusters and immature olfactory sensory neurons, and therefore fills the olfactory nerve layer in a pattern similar to that seen in Gap43 (Figure 7e). Two markers associated with the cell cycle, Ube2c (Figure 7h) and Cdk1 (not shown), identify cluster 2 cells in the olfactory nerve layer, as well as the early progenitor marker Mki67 (Figure 7i). Cluster 3 is strongly associated with OEC immune function and the expression of Apolipoprotein E (Apoe), Annexin A3 (Anxa3), and Allograft inflammatory factor 1 (Aif1/Iba1) were confirmed. Apoe (Figure 7j) is detected throughout the olfactory nerve layer and includes some cellular structures. Expression of Anxa3 (Figure 7k) and Aif1/Iba1(Figure 7l) is similar – distinct small cells labeled in the olfactory nerve layer. Our smallest group, cluster 4, has been difficult to confirm with selected antibodies targeting the top marker genes, likely due to the limited number of cells in this cluster. Overall,

our *in-situ* experiments confirmed the presence and distribution of 4 out of the 5 OEC subtypes detected by scRNA-seq.

OECs synthesize and secrete Reelin

Reelin (*Reln*) is detected in OECs in this study (Figures 2f, 8a, g) and reported in previous microarray studies (Guerout et al., 2010; Roet et al., 2011). However, the presence of the *Reln* gene within OECs is disputed in the literature (Dairaghi et al., 2018; Schnaufer et al., 2009). *Reln* codes for a large ECM glycoprotein that is secreted by neurons (D'Arcangelo et al., 1995; Kubasak et al., 2004), but also by Schwann cells (Panteri et al., 2006). In the canonical Reelin-signaling pathway, Reelin binds to the very-low-density lipoprotein receptor (Vldlr) and apolipoprotein E receptor 2 (ApoER2) and induces Src-mediated tyrosine phosphorylation of the intracellular adaptor protein Disabled-1 (Dab1). Both Reelin and Dab1 are highly expressed in embryos and contribute to correct neuronal positioning. A recent study claimed that peripheral OECs express high levels of Dab1 and Vldlr (Dairaghi et al., 2018), and that Reelin was expressed only by mesenchymal cells located near the cribriform plate, not in OECs (Dairaghi et al., 2018; Schnaufer et al., 2009). Our scRNA-seq findings of OECs demonstrated low expression levels of *Dab1* and *Apoer2* (Figure 8b-c), moderate expression of *Vldlr* (Figure 8d) and substantial levels of *Reln* in OEC subclusters 0-3 (Figure 8a). Interestingly, OECs also contain proteolytic enzymes that cleave the 400Kd secreted Reelin. Tissue plasminogen activator (tPA; Figure 8e) cleaves Reln at its C-terminus, and the matrix metalloproteinase ADAMTS-4 cuts at both the N- and C-cleavage sites of Reln (Figure 8f; Krstic et al., 2012).

The confusion about Reelin expression in OECs likely stemmed from the use of standard immunochemical methods to confirm its presence. Our attempts to detect Reelin expression in

the adult olfactory nerve layer (ONL) or in cultured OECs were unsuccessful using several antibodies and multiple protocols, despite consistent localization of Reelin within mitral cells of the olfactory bulb. To understand this discrepancy, we examined Reelin expression in embryonic sections which included both the peripheral and OB-OECs. Images of E16.5 *Reln*$^{+/+}$ olfactory system show Reelin expression in peripheral OECs and in neurons of the olfactory bulb (Figure 8g, green), but not on OB-OECs in the ONL or in sections of *Reln*$^{-/-}$ mice (Figure 8g, g2, h). In comparison, Blbp expression is uniformly expressed in the ONL of both peripheral and OB-OECs (Figure 8g1, h1, red). Enlargements of the region where axon bundles from olfactory sensory neurons join the ONL show that Blbp is present in OB-OECs throughout the ONL, but Reelin is detected only on peripheral OECs (Figure 8g, g1-2).

To determine if adult rat OB-OECs synthesize and secrete Reelin *in vitro*, we treated primary Ngfr^{p75}-purified OECs with or without Brefeldin-A, a fungal metabolite that specifically inhibits protein transport from the endoplasmic reticulum to the Golgi apparatus (Misumi et al., 1986). In Brefeldin-treated primary OEC cultures, spindle-shaped GFP-labeled OECs contain Reelin in their cytoplasm (Figure 9a, arrows). Large contaminating Reln-immunonegative cells present in primary cultures serve as an intrinsic control (Figure 9a, arrowhead). Reelin expression was also confirmed in Brefeldin-treated Ngfr^{p75}-purified OEC cultures (Figure 9b-c), a finding which supports our scRNA-seq results.

To further confirm that cultured OECs express and secrete Reelin, we performed western blotting. The G10 antibody recognizes full-length Reelin protein, which is approximately 400 kDa, and its two cleaved fragments at ~300 and ~180 kDa (Lambert de Rouvroit et al., 1999). Both the rat ONL and *Reln*$^{+/+}$ mouse olfactory bulbs showed the characteristic large molecular weight band at 400 kDa and another at 150 kDa (Figure 9d, lanes 1-2, Reln). As expected, these

bands were absent in mutant *Reln*$^{-/-}$ olfactory bulbs (Figure 9d, lane 3). Additionally, Reelin-positive bands were present in blots of OEC whole cell lysates (WCL), representing Reelin synthesized in OECs, and OEC conditioned media (CM; Figure 9d, lanes 4-8 Reln), representing Reelin secreted by OECs. A 4-15% gradient gel allowed for the visualization of all three Reelin isoforms (Figure 9e). Brain extracts of *Reln*$^{+/+}$ (positive control) and *Reln*$^{-/-}$ (negative control) mice confirm the specificity of Reelin detection (Figure 9e, lanes 1-2, 9f). All three Reelin isoforms at their corresponding molecular weights are present in rat ONL and OEC CM samples (Figure 9e, lanes 3-6, 9f). Quantification of the band densities from 4-15% gels showed that cultured OECs derived from the rat ONL and CM produce significantly higher levels of 400 and 300 kDa Reelin compared to *Reln*$^{-/-}$ mice (Figure 9f, $p<0.05$).

Discussion.

Our scRNA-seq study of immunopurified OECs identified five OEC subtypes with distinct gene expression patterns, pathways, and properties of each subtype. The well-established OEC markers are widely distributed throughout most clusters derived from cultured OECs. We also experimentally confirmed a number of the top markers at the protein level in the OEC subtypes on sections of the rat olfactory system and established that OECs secrete both Reelin and Ctgf, ECM molecules reported to be important for neural repair and axon outgrowth. Additional proregenerative OEC marker genes such as *Atf3*, *Btc*, and *Pcsk1* also were identified. Our findings provide an unbiased and in-depth view of the heterogeneity of OEC populations with demonstrated injury repair capacity, and the potential mechanisms that underlie their regenerative and protective properties.

This scRNA-seq analysis confirmed the immunopurification of the OECs compared with the mixture of OECs grown with numerous fibroblasts and microglia. Although some may debate if purified OECs are needed to maximize neural repair, this study suggests that immunopurified OECs have higher expression of anti-stress genes than unpurified controls. Several of our earlier studies, which transplanted similarly purified OECs, also showed evidence of neural regeneration following severe spinal cord injury (Khankan et al., 2016; Takeoka et al., 2011; Thornton et al., 2018). In addition to the purity of OECs, we found significant overlap of the marker genes between our study and those from the meta-analysis of five OEC microarray studies on cultured OB-OECs (Roet et al., 2011), supporting the reproducibility of our scRNA-seq findings. When we compared our data from cultured OB-OECs to previous scRNA-seq studies of the olfactory system tissue which included peripheral OECs (Durante et al, 2000), or a mixture of peripheral and OB-OECs (Tepe et al., 2018), there was little overlap. Most likely, the substantial differences were due to the dissection areas, techniques used for OEC preparation, the species studied, as well as sex and age of the subjects. It is important to note that our OB-OEC populations were repeatedly shown to induce injury repair, and their subtypes and markers support their diverse reparative functions, whereas the neural repair function of the cell populations in the other scRNA-seq studies using different tissue preparations is unclear.

OECs are hybrid glia that promote neural repair.

Based on intrinsic gene expression patterns revealed by scRNA-seq data, there is expression of select markers for Schwann cells, astrocytes, oligodendrocytes and microglia within our five clusters of OECs. We observed transcriptionally distinct clusters that highly expressed select markers for proliferation (cluster 2), microglia (cluster 3), and astrocytes and oligodendrocytes

(cluster 4). The microglia/macrophage-like cells reported by Smithson and Kawaja (2010) do resemble our transcriptome-based subtyping of OEC cluster 3. Our results further support the activities of OECs in modulating immune responses, based on the expression of genes involved in the endocytosis of bacteria, the regulation of microglia activation, and the expression of numerous lysosomal pathways (Leung et al., 2008). OECs in cluster 4 are distinctive by their expression of several astrocytic markers that regulate synaptogenesis (Thrombospondin 2) and synaptic connectivity, and remove inactive synaptic connections (Complement component 1q family; Christopherson et al., 2005; Eroglu & Barres, 2010). Additionally, our trajectory and network analyses indicate potential relationships between the OEC subclusters, which warrant further experimental testing.

Both OECs and Schwann cells originate from the neural crest, express similar immunological markers, and share many transcriptional similarities (Barraud, et al., 2010; Forni et al., 2011; Vincent et al., 2005). OECs share phenotypic characteristics with myelin-producing Schwann cells and oligodendrocytes, but more closely resemble Schwann cells (Doucette, 1991; Radtke et al., 2011; Ramon-Cueto & Valverde, 1995). Gliomedin is a required ECM protein that initiates the assembly of nodes of Ranvier along Schwann cells (Eshed et al., 2005), yet despite the fact that OECs do not have nodes of Ranvier, they express high levels of Gliomedin. This novel Gliomedin expression in OECs suggests a possible function as a glial ligand for the unmyelinated axon bundles that OECs ensheath. Following peripheral nerve injury, the loss of contact between axons and myelinating Schwann cells induces a nonmyelinating phenotypic change in Schwann cells (Fu & Gordon, 1997). These dedifferentiated nonmyelinating Schwann cells are proregenerative and upregulate the expression of Glial fibrillary acidic protein (Gfap; (Jessen et al., 1990), $Ngfr^{p75}$ receptor (You et al., 1997), cell adhesion molecules L1 and N-Cam

(Martini & Schachner, 1988), and neurotrophic factors, including Bdnf (Meyer et al., 1992) and Glial cell-line derived neurotrophic factor (Trupp et al., 1995). Genes for these proregenerative factors are detected in OECs in the present study, as well as the transcription factor *Mitf*, that controls a network of genes related to plasticity and repair in Schwann cells (Daboussi et al., 2023).

Our *in vitro* and *in vivo* experimental validation of numerous marker genes at the protein level strongly support their validity. Based on our tissue localization, the two large clusters (0 and 1) were found throughout the olfactory nerve layer, whereas cluster 2 (progenitors) and cluster 3 (microglial) are scattered within the olfactory nerve layer. Future functional studies of these subclusters will benefit from both the marker genes and their localizations uncovered in this study.

Reelin and CTGF are distinctive markers for OECs.

Reelin is a developmentally expressed protein detected in specific neurons, in addition to OECs and Schwann cells. The canonical Reelin-signaling pathway involves neuronal-secreted Reelin binding to Vldlr and ApoER2 expressed on Dab1-labeled neurons. Following Reelin binding, Dab1 is phosphorylated by Src family kinases which initiates multiple downstream pathways. Very little is known, however, about Reelin secreted by glia. Panteri et al. (2006) reported that Schwann cells express low levels of Reelin in adults, and that it is upregulated following a peripheral nerve crush, as is reported above for many neurotrophic factors. Reelin loss in Schwann cells reduced the diameter of small myelinated axons but did not affect unmyelinated axons (Panteri et al., 2005). In the olfactory system, OECs ensheath the Dab1-labeled, unmyelinated axons of olfactory sensory neurons which are continuously generated and die

throughout life. OEC transplantation following spinal cord injury would provide an exogenous source of Reelin that could phosphorylate Dab1-containing neurons or their axons. Dab1 is expressed at high levels in the axons of some projection neurons, such as the corticospinal pathway (Abadesco et al., 2014). Future experiments are needed to explore the function that glial-secreted Reelin may have on axonal regeneration.

Adult mammals show little evidence of spontaneous axonal regeneration after a severe spinal cord injury in contrast to transected neonatal rats (Bregman, 1987; Bregman et al., 1993) and young postnatal opossums (Lane et al., 2007). In immature mammals, axons continue to project across or bridge the spinal cord transection site during development. Lower organisms such as fish, show even more evidence of regeneration following severe SCI. Mokalled et al. (2016) reported that glial secretion of Ctgfα/Ccn2 was both necessary and sufficient to stimulate a glial bridge for axon regeneration across the zebrafish transection site. Cells in the injury site that express Ctgf include ependymal cells, endothelial cells, and reactive astrocytes (Conrad et al., 2005; Mokalled et al., 2016; Schwab et al., 2001). Here we show that, although rare, Ctgf-positive OECs can contribute to glial bridge formation in adult rats. The most consistent finding among our severe SCI studies combined with OEC transplantation is the extent of remodeling of the injury site and axons growing into the inhibitory lesion site, together with OECs and astrocytes. The formation of a glial bridge across the injury was critical to the spontaneous axon generation seen in zebrafish (Mokalled et al., 2016) and likely contributed to the axon regeneration detected in our OEC transplanted, transected rats (Dixie, 2019; Khankan et al., 2016; Takeoka et al., 2011; Thornton et al., 2018).

Limitations in these OEC scRNA-seq studies

We recognize that this study is a single snapshot of OEC gene expression derived from adult female rats before they are transplanted above and below the spinal cord transection site. We would expect the gene expression of transplanted OECs to change in each new environment, i.e. as they migrate into the injury site, integrate into the glial scar, and wrap around axons. Based on our past studies, OECs survived in an outbred Sprague-Dawley female rat model for ~ 4 weeks (Khankan et al., 2016) and in an inbred Fischer 344 female model for 5-6 months (Dixie, 2019). As spinal cord injury transplant procedures are further enhanced and OEC survival improves, these hybrid glial cells should be examined at multiple time points after transplantation to better evaluate their proregenerative characteristics.

We acknowledge that in humans, males account for ~80% of spinal cord injuries (National Spinal Cord Injury Statistical Center, 2024) and sustain more serious urinary tract issues than females. We examined females in the current study due to practical experimental considerations, but it is necessary to examine males in future studies. We also did not modulate any of the genes or proteins in the identified OEC subtypes to test their causal and functional roles, thus our findings remain correlative. Future gene/protein modulation studies are necessary to understand the functional roles of the individual OEC subtypes in the context of their reparative functions to determine which pathways and subtypes are more critical and can be enhanced for neural repair. Our current findings build the foundation for these future studies to help resolve the role of OECs in spinal cord injury repair.

Extensive differences between OEC preparations contribute to the large variation in results from OEC treatments following spinal cord injury. This scRNA-seq study focused entirely on OB-OECs, and the next step would be to carry out similar studies on the peripheral, lamina-propria-derived OECs to discern the differences between the two OEC populations. Such

comparative studies using scRNA-seq will help define the underlying mechanisms and resolve the variability in results from OEC-based therapy. Detailed studies of the composition of different OEC transplant types will contribute to identifying the most reparative cell transplantation treatments.

Conclusion

To understand how immunopurified OECs repair spinal cord injuries, we carried out an unbiased scRNA-seq analysis and found that OECs have a wide range of subtypes including a proliferative state, microglia-like cells and neural regenerative clusters. We demonstrated that these multi-functional OECs are clearly distinguishable from each other by expression of unique genes and pathways within subtypes based on the scRNAseq data and our *in vivo* tissue studies. These subtypes of OECs produce important ECM genes, including *Reln* and *Ctgf* and many other signaling molecules which are involved in a wide range of intercellular communication as well as axon regeneration. Our single-cell resolution investigation offers a comprehensive molecular landscape of OECs and numerous novel targets for future injury repair and functional/mechanistic studies.

Material and Methods

Animals.

All of the experimental procedures used on animals were approved by the Chancellor's Animal Research Committee at UCLA and carried out in accordance with the National Institutes of Health guidelines. Animals were housed in the Terasaki Life Science Building vivarium under standard conditions with free access to food and water.

Sprague-Dawley rats: We bred our male GFP-expressing Sprague-Dawley rats (Perry et al, 1999) with unlabeled female Sprague-Dawley rats (Charles Rivers Laboratory), which were used previously to obtain OECs from female rats for two of our spinal cord injury studies (Khankan et al., 2016; Thornton et al., 2018) in order to unambiguously identify the transplanted GFP-positive OECs near the injury sites. A total of 8, 8-10-week-old GFP-labeled female rats were used to obtain GFP-OECs for scRNA-seq. Only females were used in order to match the sex of previous SCI studies conducted exclusively on female rats (Dixie, 2019; Khankan et al., 2016; Takeoka et al., 2011; Thornton et al., 2018). Following complete thoracic spinal cord transection, an adult rat is unable to urinate voluntarily and therefore urine must be manually "expressed" twice a day throughout the experiment. Females have a shorter urethra than males, and thus their bladders are easier to empty completely. An additional 4, 8-10-week GFP-labeled rats were used to isolate Reelin protein for western blotting and 6, 8-10-week unlabeled female Sprague-Dawley rats were used to confirm gene expression in the five OEC subtypes. An overdose of ketamine-xylazine or pentobarbital was used for euthanasia before either the rat olfactory bulbs were removed or the rats were perfused with 4% paraformaldehyde or 2% PLP (2% Paraformaldehyde; 0.075M Lysine-HCL-monohydride; 0.010M Sodium periodate; 0.1M sodium phosphate) followed by a 1-2 hr postfix.

Reeler mice: To study Reelin expression in OECs, heterozygous (*Reln*$^{+/-}$) mice, originally purchased from the Jackson Laboratory (B6C3Fe-*ala-Reln*^{rl}, Bar Harbor, ME), were used for breeding. Genotypes of these mice were identified by PCR (D'Arcangelo et al., 1996). To obtain timed pregnancies, *Reln*$^{+/-}$ mice were bred and checked every morning for plugs. Pregnant mice

were heavily anesthetized with pentobarbital (100 mg/kg) and embryos were extracted at embryonic day 16.5. Heads were immersed in 2% PLP, washed in PB, cryoprotected, and embedded in Shandon M1 embedding matrix (Thermo Scientific, 1310).

Preparation of olfactory bulb-derived OEC cultures from rats and mice.

Olfactory bulbs were collected from 8-10-week-old GFP-labeled Sprague-Dawley rats or *Reln*$^{+/+}$ and *Reln*$^{-/-}$ mice. The leptomeninges were removed to reduce fibroblast contamination. Methods to prepare OEC primary cultures were adapted from Ramon-Cueto et al. (2000) and follow those reported by Runyan and Phelps (2009) for mouse OECs and Khankan et al. (2015) for rat OECs. For scRNA-seq, this protocol was replicated on two separate dates and used a total of 8 adult female Sprague-Dawley rats. Primary cultures were generated from both olfactory bulbs from each rodent. The first two layers of the olfactory bulb were dissected, isolated, and then washed in Hank's balanced salt solution (HBSS, Gibco, Rockville, MD) prior to tissue centrifugation at 365 g for 5 mins. The tissue pellet was resuspended in 0.1% trypsin and HBSS without Ca^{2+}/Mg^{2+} (Gibco, Rockville, MD), then placed in a 37°C water bath, and mixed intermittently for 10 mins. A mixture of 1:1 Dulbecco's modified eagle medium (DMEM) and Ham's F12 (D/F medium, Gibco) supplemented with 10-15% Fetal Bovine Serum (FBS, Hyclone, Logan, UT) and 1% Penicillin/Streptomycin (P/S, Gibco; D/F-FBS-P/S medium) was used to inactivate trypsin prior to centrifugation. Dissociated cells were rinsed, centrifuged 3 times, and plated into 12.5 cm^2 culture flasks pre-coated with 0.05mg/ml poly-L-lysine (PLL, Sigma, St. Louis, MO). Cells were maintained at 37°C for 5-8 days and D/F-FBS-P/S medium was changed every 2 days.

Immunopurification was carried out using hydrophobic petri dishes coated overnight with Biotin-SP-conjugated AffiniPure goat anti-rabbit IgG (1:1000; Jackson ImmunoResearch, West Grove, PA) in 50 mM Tris buffer at 4°C followed by another overnight incubation at 4°C with either mouse anti-Ngfr^{p75} for rat OECs (Suppl. Table 4, Chandler et al., 1984) or rabbit anti-Ngfr^{p75} for mouse OECs (Suppl. Table 4) in 25mM Phosphate-buffered saline (PBS). Dishes were rinsed 3 times with 25 mM PBS and treated with a mixture of PBS and 0.5% Bovine serum albumin (BSA) for 1 hr at room temperature. Prior to the addition of cells, antibody-treated dishes were washed with PBS and DMEM.

In preparation for immunopanning, two pairs of adult rat olfactory bulbs (for scRNA-seq) or four pairs of mouse bulbs (for western blots) were dissociated with 0.25% trypsin-EDTA at 37°C for 3 mins and D/F-FBS-P/S medium was added to inactivate trypsin. Following a medium rinse and centrifugation, resuspended cells were seeded onto pre-treated mouse or rabbit anti-Ngfr^{p75} petri dishes and incubated at 37°C for 10 mins. Unbound rat cells were removed with medium and saved as ‘leftover’ control cells for scRNA-seq. A cell scraper was used to recover bound cells that were then subjected to a second round of immunopanning in which purified cells from 2 rats on each experimental day were combined yielding 2 samples of purified Ngfr^{p75}-positive rat OECs and 2 samples of ‘leftover’ control cells. All cells for sequencing were replated into PLL-coated flasks. Immunopurified Ngfr^{p75}-positive mouse OECs were plated on PLL-coated 4-chamber polystrene-vessel culture slides (BD Falcon, San Jose, CA) or used for western blots. Purified OECs and ‘leftover’ controls were incubated at 37°C with 5% CO_2 for 7-8 days in D/F-FBS-P/S medium supplemented with a mitogen mixture of pituitary extract (20 μg/ml, Gibco) and forskolin (2 μM, Sigma). Media was changed every 2 days and mitogens were withdrawn 2 days prior to harvesting these cells for scRNA-seq.

Brefeldin-A treatment. Rat OECs that contained GFP could be visualized directly. Primary and purified GFP-expressing OEC cultures were rinsed 3 times with D/F medium prior to treatment with Brefeldin-A to block protein transport from the endoplasmic reticulum to the Golgi apparatus and thus block secretion. Brefeldin-A (5 μg/ml; Epicenter, Madison, WI) was mixed with D/F medium and added to OEC cultures for 2 hrs at 37ºC while the control cultures received D/F medium only. Cultures were fixed with cold 4% paraformaldehyde in 0.1 M PB for 15 mins at RT, rinsed 3 times with PBS, and stored in PBS with sodium azide at 4ºC until immunostaining.

Detection of Reelin expression in rat and mouse OEC cultures, tissue sections and western blots.

Cultured rat OECs treated with or without Brefeldin-A were labeled with mouse anti-Reelin G10 and rabbit anti-Ngfr^{p75} (Suppl. Table 4). Culture slides were rinsed with phosphate-buffered saline (PBS; 0.1M phosphate buffer; 0.9% NaCl), blocked with 5% normal goat serum for 1 h, and incubated with the appropriate primary antibodies overnight. The following day, slides were rinsed 3 times with PBS, incubated with species-appropriate Alexa Fluor 594 and/or 647 (1:500, 1:100; Jackson ImmunoResearch) for 1 hr at RT, and then cover slipped with Fluorogel (Electron Microscopy Sciences, Hatfield, PA).

Sagittal sections of the mouse E16.5 olfactory system were cut 40 μm thick, slide mounted, and stored in PB with 0.06% sodium azide. For Reelin and Blbp detection, sections were incubated overnight at RT in goat-anti-Reelin (Suppl. Table 4), rinsed thoroughly, and incubated with donkey anti-goat 488 (1:100; Jackson Immunoresearch, #705-545-0030).

Sections were then incubated in rabbit polyclonal anti-Blbp (Suppl. Table 4) overnight followed by 1 hr in donkey anti-rabbit 555 (1:800; Life Technologies, #A31572) and coverslipped with Fluorogel. Confocal images were obtained from a Zeiss Laser Scanning Microscope (LSM800) with solid-state lasers 488 and 561 nm for double-labeled images.

Tissue harvesting, protein isolation, and western blotting. Olfactory bulbs from adult *Reln*$^{+/+}$ and *Reln*$^{-/-}$ mice and olfactory nerve layers from adult Sprague Dawley rats were freshly dissected as described for primary OEC cultures. Olfactory tissue was collected, placed on ice, and homogenized in Ripa lysis buffer plus protease inhibitor cocktail (Sigma). Protein concentrations of brain and olfactory extracts were determined using the RC DC Protein Assay kit (Bio-Rad, Hercules, CA) as described (Miller et al., 2008). Whole-cell lysates (WCL) and conditioned medium (CM) were obtained from purified OEC cultures maintained in D/F medium. CM was collected from OEC cultures before cells were incubated with Ripa lysis buffer and collected with a cell scraper. Protein samples were stored at -80ºC.

Protein samples (50 μg) were heated to 90–100°C for 3 mins, resolved on 10% SDS-PAGE or 4–15% mini-protean TGX gels (Bio-Rad) run in Tris-Glycine-SDS (TGS) buffer (Bio-Rad) at 60V, and then transferred onto 0.22 μm PVDF/nitrocellulose membranes (Bio-Rad) in TGS with 20% methanol at 25V overnight at 4°C. Precision plus protein standards in dual color (Bio-Rad) were used to determine molecular weight. Membranes were cut, blocked with 5% non-fat dry skimmed milk (Bio-Rad) in Tris-buffered saline containing 0.1% Tween-20 (TBST) for 1 hr at room temperature on a shaker, and then incubated overnight at 4°C TBST plus 2.5% milk containing anti-Reelin G10 or loading control mouse anti-GAPDH antibodies (Suppl. Table 4). Following primary antibody incubation, blots were washed 3 times in TBST for 10 mins

while shaking and then probed with horseradish peroxidase-conjugated secondary anti-mouse IgG (1:2,000 for Reelin, 1:5,000 for GAPDH) in TBST. Immunoblots were developed using a chemiluminescence HRP detection kit (GE Healthcare, Piscataway, NJ,) and imaged with a Typhoon scanner (GE Healthcare).

For quantification, ImageJ software (NIH) was used to analyze the densitometric data. Western blot images at 400, 300, and 150 kDa resolution were converted to grayscale followed by manually defining a Region of Interest (ROI) frame that captured the entire band in each lane using the "Rectangular" tool. The area of each selected band was measured by employing the same ROI frame around the band to record the integrated density, "Grey Mean Value". Background measurements were similarly quantified, and background subtraction was performed by deducting the inverted background from the inverted band value. For relative quantification, target protein bands were normalized to the corresponding loading control (GAPDH) to derive normalized protein expression (fold change). Band intensities were quantified in triplicate for each sample. Data were analyzed with the Mann-Whitney U test to compare normalized protein expression between the *Reln*$^{-/-}$ group and the other groups. A one-sided p-value was calculated to test the hypothesis that protein expression levels in the other groups are greater than those in the *Reln*$^{-/-}$ group. Statistical significance was determined at $p < 0.05$. Analysis was performed using GraphPad Prism (version 9).

Single-cell RNA-sequencing

Cell collection and culture. Flasks with purified OECs and leftover cells were rinsed with HBSS and dissociated with trypsin-EDTA as above. Cells were washed in D/F-FBS-P/S medium and further resuspended with siliconized pipettes. Media and cells were washed and centrifuged at

365 *g* for 10 min, and resuspended. After the final wash, cells for sequencing were resuspended in PBS+BSA in volumes of 1200 cells/µL. On each of 2 different culture days, 4 flasks of cells (2 purified OECs and 2 'leftovers') were generated for scRNA-seq, yielding 8 samples in total (4 purified OECs and 4 'leftovers'). To confirm our scRNA-seq results directly with immunocytochemistry, we plated extra cells from the second preparation on PLL-coated coverslips in 24-well plates with 500µL D/F-FBS-P/S medium. Medium was changed at 2 days, cultures were fixed at 3 days in cold 4% paraformaldehyde for 20 mins, washed 3X with PB and stored in PB with 0.06% sodium azide.

scRNA-seq was performed using the 10X Genomics Chromium scRNA-seq system which incorporates microfluidic capture-based encapsulation, barcoding, and library preparation (10X Genomics, Pleasanton, CA). About 10,000 cells per OEC or leftover preparation were loaded into a Chromium Chip B along with partitioning oil, reverse transcription reagents, and a mix of hydrogel beads containing 3,500,000 unique 10X barcodes. Paired-end sequencing was performed on a Novaseq S4 system, using the v3 Illumina platform, at 20-50K reads/cell. The paired-end reads were processed using the Cell Ranger pipeline and *Rattus norvegicus* (Rnor_6.0) from Ensembl as the reference genome (Yates et al., 2020) to produce a gene expression matrix. Among the 8 samples, one OEC sample showed a low fraction of reads and RNA content in cells, which may indicate high level of ambient RNA (Suppl. Figure 3a). This sample was removed from further analysis, leaving 3 OEC samples and 4 leftover samples for downstream analysis.

scRNA-seq data quality control, normalization, and integration. Gene expression matrix from each of the 7 remaining samples that passed quality control was loaded into the Seurat R package

ver 3.0 (Stuart et al., 2019). Cells were called based on the number of genes (200-5000), unique molecular identifiers (UMIs; 5000-20000), and percent of mitochondrial genes (<20%; Suppl. Figure 3b). After quality control, log normalization was performed within each sample using *NormalizeData* function with default parameters. Top 2,000 variable genes were selected using *FindVariableFeatures*. The seven samples were integrated together with *FindIntegrationAnchors* and *IntegrateData* functions which incorporate canonical correlation analysis to align cells with similar transcriptomic patterns across samples.

Cell clustering and cell type identification. The integrated Seurat object was used for the principal component analysis (PCA). The top 15 PCs were used to construct the k-nearest neighbor graph, followed by Louvain algorithm to cluster cells based on similar gene expression patterns. Cell clusters were visualized using tSNE plots.

To assign cell type identities to each cluster, marker genes of each cluster were found using *FindAllMarkers* with average log fold change > 0.5 and minimum percent difference > 0.25. Cell cluster marker genes were subsequently compared to known OEC cell type markers curated from previous studies that used different species, sex, age, dissection areas, and cell preparation methods (Durante et al., 2020; Tepe et al., 2018). Additional marker genes for fibroblasts and multiple glial cell types including astrocytes, oligodendrocytes, and microglia were also used to compare with those of the cell clusters. Cell clusters whose marker genes match known cell type markers were labeled with the corresponding cell type identity. Gene expression heatmaps of top markers were generated to visualize the distinct expression patterns of the marker genes for different cell clusters.

OEC subtype identification. A subset of cells expressing well-known OEC markers (e.g., *Ngfr*^{p75}, *S100β*, and *Sox10*) was labeled as OECs and then selected for further subclustering analysis to identify potential OEC subtypes. To do this, OECs from the original Seurat object were extracted using the *subset* function and the top 10 PCs of each OEC subset were used for clustering analysis and tSNE visualization. Marker genes for each OEC subcluster were identified using the *FindAllMarkerGene* function. Pseudotime trajectory analysis across the OEC subtypes was performed using Slingshot version 1.8.0 (Street et al., 2018).

Pathway enrichment analysis. To annotate the biological functions of the marker genes of individual cell clusters or OEC subclusters, we carried out pathway enrichment analysis using EnrichR ver 3.0, where KEGG, Reactome, and GO Biological Process were used as reference pathway databases (Chen et al., 2013). Top pathways were ranked by multiple-testing adjusted P-values.

Potential cell-cell ligand-receptor interactions across OEC subtypes. In order to characterize potential interactions mediated by secreted ligand-receptor pairs between subtypes of OECs, we implemented NicheNet (Browaeys et al., 2020), which curates ligand-receptor interactions from various publicly available resources. The NicheNet ligand-receptor model was integrated with markers from each OEC subtype to find potentially activated ligand-receptor pairs. Differentially expressed ligands identified by markers from source OEC subtypes and activated receptors identified by NicheNet in target OEC subtypes were used to assess ligand-receptor interaction. Ligand-receptor interaction networks between cell types were visualized using Cytoscape (Shannon et al., 2003).

Confirmation of OEC gene expression *in vitro* and *in vivo*.

Immunocytochemistry experiments to confirm gene expression revealed by scRNA-seq were conducted on extra cultured OECs and 'leftover' controls which were replated and cultured for 3 additional days. OECs samples were treated with the following primary antibodies against OEC marker genes identified from scRNA-seq with experimental parameters recorded in Suppl. Table 4: 1) polyclonal and monoclonal anti-Blbp, 2) anti-N-Cadherins, 3) anti-green fluorescent protein, 4) anti-Ki67, 5) anti-L1, 6) anti-NCAM, 7) monoclonal anti-Ngfr^{p75}, 8) anti-S100β, and 9) anti-SOX10. Prior to adding the primary antibodies, the cells were incubated in 0.3% Triton-X 100 detergent in PBS. Cells were blocked in 5% normal donkey serum (Jackson ImmunoResearch Laboratories, # 017-000-121) with 0.3% Triton-X before adding the primary antibodies and left to incubate at RT overnight on the rotator. Following multiple washes, species-appropriate secondary antibodies with fluorescence for 488, 555, and 647 were used to visualize the immunoreaction (1:200 – 1:500, Jackson ImmunoResearch Labs donkey-anti-chicken-488, # 703-545-155; donkey-anti-rabbit-647, # 711-605-152; donkey-anti-mouse-647, # 715-605-150; Life Technologies, donkey-anti-mouse-555, # A31570; donkey-anti-rabbit-555, # A31572). Cultures were counterstained with Hoechst (Bis-benzimide, 1:500, Sigma-Aldrich, # B2261) and coverslipped with EverBrite medium (Biotium, # 23001).

To examine Ctgf expression in the spinal cord lesion site, we processed 1 slide per animal with ~6 equally-spaced sagittal sections (25 µm thick) throughout spinal cords from the Khankan et al. (2016) study. Our aim was to assess if transplanted OECs (n=4 rats) and transplanted fibroblasts (n=3 rats) express Ctgf in the injury site.

Experiments were carried out to confirm gene expression of OEC subtype markers in the 8-10-week-old olfactory system of rats. Soft tissues and the jaw were removed from fixed heads that were decalcified in undiluted formic acid bone decalcifier (Immunocal, Decal Chemical Corps, Tallman, NY) for 12 hrs., washed, and then infiltrated with increasing concentrations of 5% to 20% sucrose for 24 hr. Heads in 20% sucrose were heated in a 37°C oven and then placed in a gelatin sucrose mixture for 4 hrs, embedded in warm gelatin sucrose in a plastic mold, allowed to gel, frozen on dry ice and stored at -70°C. Heads were sectioned coronally at 40 µm thick, and mounted in series on 16 glass slides. Several antibodies from each of the 4 OEC clusters were chosen to determine their distribution in olfactory bulb sections. Primary antibodies used are listed in Suppl. Table 4, together with the experimental parameters used. For most antibodies, the olfactory bulb sections first underwent a heat-induced antigen retrieval step with 10mM citric acid at pH 6 for 5 min and then were transferred to 1.5% NDS and 0.1% Triton-X-100 in TBS-BSA (0.1M Tris; 1.4% NaCl; 0.1% BSA) for 1 h followed by overnight incubation in primary antibody at RT. Following multiple washes, species-appropriate secondary antibodies with fluorescence for 488 and 555 were used to visualize the immunoreactivity.

For experiments carried out using a Tyramide Signal Amplification (TSA) kit, sections were first incubated in 1% hydrogen peroxide and 0.1% sodium azide in phosphate-buffered saline PBS for 30 mins followed by 10% NDS and 0.1% Triton X-100 in PBS for 1 hr. Next, the sections were incubated with Avidin-Biotin solution (Vector laboratories; kit #SP-2001) before an overnight incubation with the primary antibody at RT. The next day, sections were washed in PBS followed by TNT buffer (0.1M Tris-HCl; 0.15M NaCl; 0.05% Tween) and then a 1 hr incubation with biotinylated horse anti-goat IgG (1:1000; Vector laboratories; #BA-9500), biotinylated donkey anti-rabbit IgG (1:1000; Jackson Immunoresearch; #711-065-152), or

biotinylated donkey anti-mouse IgG (1:1000; Jackson Immunoresearch; #715-065-150) in TSA-specific blocking buffer (TNB; 0.1M Tris-HCl; 0.15M NaCl; 0.5% Blocking reagent; PerkinElmer; #FP1020). Sections were then washed with TNT followed by a 1 h incubation with streptavidin-conjugated horseradish peroxidase (1:1000; PerkinElmer; #NEL750001EA) in TNB, and a 10-min incubation with TSA Plus Fluorescein (1:150; PerkinElmer; #NEL741001KT) or TSA Plus Cyanine 3 (Cy3; 1:100; PerkinElmer; #NEL744001KT). Sections were imaged on an Olympus AX70 microscope with a Zeiss AxioCam HRcRv.2 camera. Images were transferred to Adobe Photoshop for assembly, cropping, and adjustment of brightness/contrast to create the compiled figures.

Morphological analyses of Ki67 OEC subtypes

To determine if OEC progenitor cells marked with Ki67 immunoreactivity have a distinctive morphology, purified and fixed OEC cultures from four rats were processed with anti-Ngfr^{p75}, anti-Ki67 and counterstained with Hoechst (Bis-benzimide, 1:500, Sigma-Aldrich, #B2261). Images were acquired from 7-10 randomly selected fields/sample using an Olympus AX70 microscope and Zen image processing and analysis software (Carl Zeiss). We distinguished the larger, flat ‘astrocyte-like’ OECs from the smaller, fusiform ‘Schwann cell-like’ OECs, and recorded their expression of Ngfr^{p75} and Ki67. Cell counts from each field were averaged per rat and then averaged into a group mean ± SEM. A Student t-test was conducted to compare the effect of Ngfr^{p75}-labeled cell morphology and the proliferative marker Ki67. Statistical significance was determined by $p < 0.05$.

References

Abadesco, A. D., Cilluffo, M., Yvone, G. M., Carpenter, E. M., Howell, B. W., & Phelps, P. E. (2014). Novel Disabled-1-expressing neurons identified in adult brain and spinal cord. *Eur J Neurosci*, *39*(4), 579-592. https://doi.org/10.1111/ejn.12416

Asan, E., Langenhan, T., Holtmann, B., Bock, H., Sendtner, M., & Carroll, P. (2003). Ciliary neurotrophic factor in the olfactory bulb of rats and mice. *Neuroscience*, *120*(1), 99-112. https://doi.org/10.1016/s0306-4522(03)00211-2

Barraud, P., Seferiadis, A. A., Tyson, L. D., Zwart, M. F., Szabo-Rogers, H. L., Ruhrberg, C., Liu, K. J. & Baker, C. V. H. (2010). Neural crest origin of olfactory ensheathing glia. *Proc. Natl. Acad. Sci. U.S.A.* 107, 21040-21045. https://onlinelibrary.wiley.com/doi/full/10.1002/glia.23870

Boekhoorn, K., van Dis, V., Goedknegt, E., Sobel, A., Lucassen, P. J., & Hoogenraad, C. C. (2014). The microtubule destabilizing protein stathmin controls the transition from dividing neuronal precursors to postmitotic neurons during adult hippocampal neurogenesis. *Dev Neurobiol*, *74*(12), 1226-1242. https://doi.org/10.1002/dneu.22200

Bregman, B. S. (1987) Spinal cord transplants permit the growth of serotonergic axons across the site of neonatal spinal cord transection. *Dev Brain Res 43*(2), 265-270. https//doi.org/10.1016/0165-3806(87)90214-8

Bregman, B. S., Kunkel-Bagden, E., Reier, P. J., Dai, H. N., McAtee, M., and Gao, D. (1993) Recovery of function after spinal cord injury: Mechanisms underlying transplant-mediated recovery of function differ after spinal cord injury in newborn and adult rats. *Expt Neurol 123*(1),3-16. https://doi.org/10.1006/exnr.1993.1136

Browaeys, R., Saelens, W., & Saeys, Y. (2020). NicheNet: modeling intercellular communication by linking ligands to target genes. *Nat Methods*, *17*(2), 159-162. https://doi.org/10.1038/s41592-019-0667-5

Burda, J. E., & Sofroniew, M. V. (2014). Reactive gliosis and the multicellular response to CNS damage and disease. *Neuron*, *81*(2), 229-248. https://doi.org/10.1016/j.neuron.2013.12.034

Chandler, C. E., Parsons, L. M., Hosang, M., & Shooter, E. M. (1984). A monoclonal antibody modulates the interaction of nerve growth factor with PC12 cells. *J Biol Chem*, *259*(11), 6882-6889. https://www.ncbi.nlm.nih.gov/pubmed/6327698

Chen, E. Y., Tan, C. M., Kou, Y., Duan, Q., Wang, Z., Meirelles, G. V., Clark, N. R., & Ma'ayan, A. (2013). Enrichr: interactive and collaborative HTML5 gene list enrichment analysis tool. *BMC Bioinformatics*, *14*, 128. https://doi.org/10.1186/1471-2105-14-128

Christopherson, K. S., Ullian, E. M., Stokes, C. C., Mullowney, C. E., Hell, J. W., Agah, A., Lawler, J., Mosher, D. F., Bornstein, P., & Barres, B. A. (2005). Thrombospondins are astrocyte-secreted proteins that promote CNS synaptogenesis. *Cell*, *120*(3), 421-433. https://doi.org/10.1016/j.cell.2004.12.020

Chung, R. S., Woodhouse, A., Fung, S., Dickson, T. C., West, A. K., Vickers, J. C., & Chuah, M. I. (2004). Olfactory ensheathing cells promote neurite sprouting of injured axons in vitro by direct cellular contact and secretion of soluble factors. *Cell Mol Life Sci*, *61*(10), 1238-1245. https://doi.org/10.1007/s00018-004-4026-y

Conrad, S., Schluesener, H. J., Adibzahdeh, M., & Schwab, J. M. (2005). Spinal cord injury induction of lesional expression of profibrotic and angiogenic connective tissue growth

factor confined to reactive astrocytes, invading fibroblasts and endothelial cells. *J Neurosurg Spine*, *2*(3), 319-326. https://doi.org/10.3171/spi.2005.2.3.0319

Cregg, J. M., DePaul, M. A., Filous, A. R., Lang, B. T., Tran, A., & Silver, J. (2014). Functional regeneration beyond the glial scar. *Exp Neurol*, *253*, 197-207. https://doi.org/10.1016/j.expneurol.2013.12.024

D'Arcangelo, G., Miao, G. G., Chen, S. C., Soares, H. D., Morgan, J. I., & Curran, T. (1995). A protein related to extracellular matrix proteins deleted in the mouse mutant reeler. *Nature*, *374*(6524), 719-723. https://doi.org/10.1038/374719a0

D'Arcangelo, G., Miao, G. G., & Curran, T. (1996). Detection of the reelin breakpoint in reeler mice. *Brain Res Mol Brain Res*, *39*(1-2), 234-236. https://doi.org/10.1016/0169-328x(96)00046-0

Daboussi, L., Costaguta, G., Gullo, M., Jasinski, N., Pessino, V., O'Leary, B., Lettieri, K., Driscoll, S., & Pfaff, S. L. (2023). Mitf is a Schwann cell sensor of axonal integrity that drives nerve repair. *Cell Rep*, *42*(11), 113282. https://doi.org/10.1016/j.celrep.2023.113282

Dairaghi, L., Flannery, E., Giacobini, P., Saglam, A., Saadi, H., Constantin, S., Casoni, F., Howell, B. W., & Wray, S. (2018). Reelin can modulate migration of olfactory ensheathing cells and Gonadotropin releasing hormone neurons via the canonical pathway. *Front Cell Neurosci*, *12*, 228. https://doi.org/10.3389/fncel.2018.00228

Dixie, K. L. I. (2019). Transplantation of olfactory ensheathing cells combined with epidural stimulation and climb training as a long-term treatment for severe spinal cord injury in rodents. *UCLA. ProQuest ID, Dixie_ucla_0031D_18445. Merritt ID: ark:/13030/m5ps32vp*.

Doucette, R. (1990). Glial influences on axonal growth in the primary olfactory system. *Glia*, *3*(6), 433-449. https://doi.org/10.1002/glia.440030602

Doucette, R. (1991). PNS-CNS transitional zone of the first cranial nerve. *J Comp Neurol*, *312*(3), 451-466. https://doi.org/10.1002/cne.903120311

Durante, M. A., Kurtenbach, S., Sargi, Z. B., Harbour, J. W., Choi, R., Kurtenbach, S., Goss, G. M., Matsunami, H., & Goldstein, B. J. (2020). Single-cell analysis of olfactory neurogenesis and differentiation in adult humans. *Nat Neurosci*, *23*(3), 323-326. https://doi.org/10.1038/s41593-020-0587-9

Eroglu, C., & Barres, B. A. (2010). Regulation of synaptic connectivity by glia. *Nature*, *468*(7321), 223-231. https://doi.org/10.1038/nature09612

Eshed, Y., Feinberg, K., Poliak, S., Sabanay, H., Sarig-Nadir, O., Spiegel, I., Bermingham, J. R., Jr., & Peles, E. (2005). Gliomedin mediates Schwann cell-axon interaction and the molecular assembly of the nodes of Ranvier. *Neuron*, *47*(2), 215-229. https://doi.org/10.1016/j.neuron.2005.06.026

Forni, P. E., Taylor-Burds, C., Melvin, V. S., Williams, T., & Wray, S. (2011). Neural crest and ectodermal cells intermix in the nasal placode to give rise to GnRH-1 neurons, sensory neurons, and olfactory ensheathing cells. *J Neurosci*, *31*(18), 6915-6927. https://doi.org/10.1523/JNEUROSCI.6087-10.2011

Franceschini, I. A., & Barnett, S. C. (1996). Low-affinity NGF-receptor and E-N-CAM expression define two types of olfactory nerve ensheathing cells that share a common lineage. *Dev Biol*, *173*(1), 327-343. https://doi.org/10.1006/dbio.1996.0027

Franssen, E. H. P., de Bree, F. M., & Verhaagen, J. (2007) Olfactory ensheathing glia: Their

contribution to primary olfactory nervous system regeneration and their regenerative potential following transplantation into the injured spinal cord. *Brain Res Reviews 56*, 236-258. https://doi.org/10.1016/j.brainresrev.2007.07.013

Fu, S. Y., & Gordon, T. (1997). The cellular and molecular basis of peripheral nerve regeneration. *Mol Neurobiol*, *14*(1-2), 67-116. https://doi.org/10.1007/BF02740621

Granger, N., Blamires, H., Franklin, R. J., & Jeffery, N. D. (2012). Autologous olfactory mucosal cell transplants in clinical spinal cord injury: a randomized double-blinded trial in a canine translational model. *Brain*, *135*(Pt 11), 3227-3237. https://doi.org/10.1093/brain/aws268

Graziadei, P. P., & Monti Graziadei, G. A. (1985). Neurogenesis and plasticity of the olfactory sensory neurons. *Ann N Y Acad Sci*, *457*, 127-142. https://doi.org/10.1111/j.1749-6632.1985.tb20802.x

Gresle, M. M., Butzkueven, H., Perreau, V. M., Jonas, A., Xiao, J., Thiem, S., Holmes, F. E., Doherty, W., Soo, P. Y., Binder, M. D., Akkermann, R., Jokubaitis, V. G., Cate, H. S., Marriott, M. P., Gundlach, A. L., Wynick, D., & Kilpatrick, T. J. (2015). Galanin is an autocrine myelin and oligodendrocyte trophic signal induced by leukemia inhibitory factor. *Glia*, *63*(6), 1005-1020. https://doi.org/10.1002/glia.22798

Guerout, N., Derambure, C., Drouot, L., Bon-Mardion, N., Duclos, C., Boyer, O., & Marie, J. P. (2010). Comparative gene expression profiling of olfactory ensheathing cells from olfactory bulb and olfactory mucosa. *Glia*, *58*(13), 1570-1580. https://doi.org/10.1002/glia.21030

Hunt, D., Hossain-Ibrahim, K., Mason, M. R., Coffin, R. S., Lieberman, A. R., Winterbottom, J., & Anderson, P. N. (2004). ATF3 upregulation in glia during Wallerian degeneration: differential expression in peripheral nerves and CNS white matter. *BMC Neurosci*, *5*, 9. https://doi.org/10.1186/1471-2202-5-9

Ingram, N. T., Khankan, R. R., & Phelps, P. E. (2016). Olfactory ensheathing cells express alpha7 integrin to mediate their migration on laminin. *PLoS One*, *11*(4), e0153394. https://doi.org/10.1371/journal.pone.0153394

Jessen, K. R., Morgan, L., Stewart, H. J., & Mirsky, R. (1990). Three markers of adult non-myelin-forming Schwann cells, 217c(Ran-1), A5E3 and GFAP: development and regulation by neuron-Schwann cell interactions. *Development*, *109*(1), 91-103. https://doi.org/10.1242/dev.109.1.91

Khankan, R. R., Griffis, K. G., Haggerty-Skeans, J. R., Zhong, H., Roy, R. R., Edgerton, V. R., & Phelps, P. E. (2016). Olfactory ensheathing cell transplantation after a complete spinal cord transection mediates neuroprotective and immunomodulatory mechanisms to facilitate regeneration. *J Neurosci*, *36*(23), 6269-6286. https://doi.org/10.1523/JNEUROSCI.0085-16.2016

Khankan, R. R., Wanner, I. B., & Phelps, P. E. (2015). Olfactory ensheathing cell-neurite alignment enhances neurite outgrowth in scar-like cultures. *Exp Neurol*, *269*, 93-101. https://doi.org/10.1016/j.expneurol.2015.03.025

Krstic, D., Rodriguez, M., & Knuesel, I. (2012). Regulated proteolytic processing of Reelin through interplay of tissue plasminogen activator (tPA), ADAMTS-4, ADAMTS-5, and their modulators. *PLoS One*, *7*(10), e47793. https://doi.org/10.1371/journal.pone.0047793

Kubasak, M. D., Brooks, R., Chen, S., Villeda, S. A., & Phelps, P. E. (2004). Developmental distribution of Reelin-positive cells and their secreted product in the rodent spinal cord. *J Comp Neurol*, *468*(2), 165-178. https://doi.org/10.1002/cne.10946

Lakatos, A., Barnett, S. C., & Franklin, R. J. (2003). Olfactory ensheathing cells induce less host astrocyte response and chondroitin sulphate proteoglycan expression than Schwann cells following transplantation into adult CNS white matter. *Exp Neurol*, *184*(1), 237-246. https://doi.org/10.1016/s0014-4886(03)00270-x

Lakatos, A., Franklin, R. J., & Barnett, S. C. (2000). Olfactory ensheathing cells and Schwann cells differ in their in vitro interactions with astrocytes. *Glia*, *32*(3), 214-225. https://doi.org/10.1002/1098-1136(200012)32:3

Lambert de Rouvroit, C., de Bergeyck, V., Cortvrindt, C., Bar, I., Eeckhout, Y., & Goffinet, A. M. (1999). Reelin, the extracellular matrix protein deficient in reeler mutant mice, is processed by a metalloproteinase. *Exp Neurol*, *156*(1), 214-217. https://doi.org/10.1006/exnr.1998.7007

Lamond, R., & Barnett, S. C. (2013). Schwann cells but not olfactory ensheathing cells inhibit CNS myelination via the secretion of connective tissue growth factor. *J Neurosci*, *33*(47), 18686-18697. https://doi.org/10.1523/JNEUROSCI.3233-13.2013

Lane, M. A., Truettner, J. S., Brunschwig, J-P., Gomez, A., Bunge, M. B., Dietrich, W. D., Dziegielewska, K. M., Ek, C. J., VandeBerg, J. L., & Saunders, N. R. (2007) Age-related differences in the local cellular and molecular responses to injury in developing spinal cord of the opossum, *Monodelphis domestica*. *Eur J Neurosci 25(6)*, 1725-1742. https://doi.org/10.1111/j.1460-9568.2007.05439.x

Leung, J. Y., Chapman, J. A., Harris, J. A., Hale, D., Chung, R. S., West, A. K., & Chuah, M. I. (2008). Olfactory ensheathing cells are attracted to, and can endocytose, bacteria. *Cell Mol Life Sci*, *65*(17), 2732-2739. https://doi.org/10.1007/s00018-008-8184-1

Li, Y., Li, D., & Raisman, G. (2005). Interaction of olfactory ensheathing cells with astrocytes may be the key to repair of tract injuries in the spinal cord: the 'pathway hypothesis'. *J Neurocytol*, *34*(3-5), 343-351. https://doi.org/10.1007/s11068-005-8361-1

Martini, R., & Schachner, M. (1988). Immunoelectron microscopic localization of neural cell adhesion molecules (L1, N-CAM, and myelin-associated glycoprotein) in regenerating adult mouse sciatic nerve. *J Cell Biol*, *106*(5), 1735-1746. https://doi.org/10.1083/jcb.106.5.1735

Meyer, M., Matsuoka, I., Wetmore, C., Olson, L., & Thoenen, H. (1992). Enhanced synthesis of brain-derived neurotrophic factor in the lesioned peripheral nerve: different mechanisms are responsible for the regulation of BDNF and NGF mRNA. *J Cell Biol*, *119*(1), 45-54. https://doi.org/10.1083/jcb.119.1.45

Miller, J. E., Spiteri, E., Condro, M. C., Dosumu-Johnson, R. T., Geschwind, D. H., & White, S. A. (2008). Birdsong decreases protein levels of FoxP2, a molecule required for human speech. *J Neurophysiol*, *100*(4), 2015-2025. https://doi.org/10.1152/jn.90415.2008

Misumi, Y., Misumi, Y., Miki, K., Takatsuki, A., Tamura, G., & Ikehara, Y. (1986). Novel blockade by brefeldin A of intracellular transport of secretory proteins in cultured rat hepatocytes. *J Biol Chem*, *261*(24), 11398-11403. https://www.ncbi.nlm.nih.gov/pubmed/2426273

Mokalled, M. H., Patra, C., Dickson, A. L., Endo, T., Stainier, D. Y., & Poss, K. D. (2016). Injury-induced ctgfa directs glial bridging and spinal cord regeneration in zebrafish. *Science*, *354*(6312), 630-634. https://doi.org/10.1126/science.aaf2679

Nakhjavan-Shahraki, B., Yousefifard, M., Rahimi-Movaghar, V., Baikpour, M., Nasirinezhad, F., Safari, S., Yaseri, M., Jafari, A. M., Ghelichkhani, P., Tafakhori, A. & Hosseini, M. (2018) Transplantation of olfactory ensheathing cells on functional recovery and

neuropathic pain after spinal cord injury; systematic review and meta-analysis. *Scientific Reports* 8:325. https://doi.10.1038/s41598-017-18754-4

National Spinal Cord Statistical Center. (2024) Traumatic Spinal Cord Injury Facts and Figures at a Glance -2024. https://sites.uab.edu/nscisc/

Nazareth, L., Lineburg, K. E., Chuah, M. I., Tello Velasquez, J., Chehrehasa, F., St John, J. A., & Ekberg, J. A. (2015). Olfactory ensheathing cells are the main phagocytic cells that remove axon debris during early development of the olfactory system. *J Comp Neurol*, *523*(3), 479-494. https://doi.org/10.1002/cne.23694

Nazareth, L., Shelper, T. B., Chacko, A., Basu, S., Delbaz, A., Lee, J. Y. P., Chen, M., St John, J. A., & Ekberg, J. A. K. (2020). Key differences between olfactory ensheathing cells and Schwann cells regarding phagocytosis of necrotic cells: implications for transplantation therapies. *Sci Rep*, *10*(1), 18936. https://doi.org/10.1038/s41598-020-75850-8

Panteri, R., Mey, J., Zhelyaznik, N., D'Altocolle, A., Fa`, A. D., Gangitano, C. M., Marino, R., Lorenzetto, E., Buffelli, M., and Keller, F. (2006). Reelin is transiently expressed in the peripheral nerve during development and is upregulated following nerve crush. *Mol. Cell. Neurosci.*, *32*, 133-142. https://doi.org/10.1016/j.mcn.2006.03.004

Radtke, C., Sasaki, M., Lankford, K. L., Gallo, V., & Kocsis, J. D. (2011). CNPase expression in olfactory ensheathing cells. *J Biomed Biotechnol*, *2011*, 608496. https://doi.org/10.1155/2011/608496

Ramon-Cueto, A., Cordero, M. I., Santos-Benito, F. F., & Avila, J. (2000). Functional recovery of paraplegic rats and motor axon regeneration in their spinal cords by olfactory ensheathing glia. *Neuron*, *25*(2), 425-435. https://doi.org/10.1016/s0896-6273(00)80905-8

Ramon-Cueto, A., & Valverde, F. (1995). Olfactory bulb ensheathing glia: a unique cell type with axonal growth-promoting properties. *Glia*, *14*(3), 163-173. https://doi.org/10.1002/glia.440140302

Roet, K. C., Bossers, K., Franssen, E. H., Ruitenberg, M. J., & Verhaagen, J. (2011). A meta-analysis of microarray-based gene expression studies of olfactory bulb-derived olfactory ensheathing cells. *Exp Neurol*, *229*(1), 10-45. https://doi.org/10.1016/j.expneurol.2011.03.001

Ruitenberg, M. J., Plant, G. W., Hamers, F. P., Wortel, J., Blits, B., Dijkhuizen, P. A., Gispen, W. H., Boer, G. J., & Verhaagen, J. (2003). Ex vivo adenoviral vector-mediated neurotrophin gene transfer to olfactory ensheathing glia: effects on rubrospinal tract regeneration, lesion size, and functional recovery after implantation in the injured rat spinal cord. *J Neurosci*, *23*(18), 7045-7058. https://www.ncbi.nlm.nih.gov/pubmed/12904465

Runyan, S. A., & Phelps, P. E. (2009). Mouse olfactory ensheathing glia enhance axon outgrowth on a myelin substrate in vitro. *Exp Neurol*, *216*(1), 95-104. https://doi.org/10.1016/j.expneurol.2008.11.015

Sasaki, M., Black, J. A., Lankford, K. L., Tokuno, H. A., Waxman, S. G., & Kocsis, J. D. (2006). Molecular reconstruction of nodes of Ranvier after remyelination by transplanted olfactory ensheathing cells in the demyelinated spinal cord. *J Neurosci*, *26*(6), 1803-1812. https://doi.org/10.1523/JNEUROSCI.3611-05.2006

Schnaufer, C., Breer, H., & Fleischer, J. (2009). Outgrowing olfactory axons contain the Reelin receptor VLDLR and navigate through the Reelin-rich cribriform mesenchyme. *Cell Tissue Res*, *337*(3), 393-406. https://doi.org/10.1007/s00441-009-0762-5

Schwab, J. M., Beschorner, R., Nguyen, T. D., Meyermann, R., & Schluesener, H. J. (2001). Differential cellular accumulation of connective tissue growth factor defines a subset of reactive astrocytes, invading fibroblasts, and endothelial cells following central nervous system injury in rats and humans. *J Neurotrauma*, *18*(4), 377-388. https://doi.org/10.1089/089771501750170930

Shannon, P., Markiel, A., Ozier, O., Baliga, N. S., Wang, J. T., Ramage, D., Amin, N., Schwikowski, B., & Ideker, T. (2003). Cytoscape: a software environment for integrated models of biomolecular interaction networks. *Genome Res*, *13*(11), 2498-2504. https://doi.org/10.1101/gr.1239303

Smithson, L. J., & Kawaja, M. D. (2010). Microglial/macrophage cells in mammalian olfactory nerve fascicles. *J Neurosci Res*, *88*(4), 858-865. https://doi.org/10.1002/jnr.22254

Street, K., Risso, D., Fletcher, R. B., Das, D., Ngai, J., Yosef, N., Purdom, E., & Dudoit, S. (2018). Slingshot: cell lineage and pseudotime inference for single-cell transcriptomics. *BMC Genomics*, *19*(1), 477. https://doi.org/10.1186/s12864-018-4772-0

Stuart, T., Butler, A., Hoffman, P., Hafemeister, C., Papalexi, E., Mauck, W. M., 3rd, Hao, Y., Stoeckius, M., Smibert, P., & Satija, R. (2019). Comprehensive integration of single-cell data. *Cell*, *177*(7), 1888-1902 e1821. https://doi.org/10.1016/j.cell.2019.05.031

Su, Z., Chen, J., Qiu, Y., Yuan, Y., Zhu, F., Zhu, Y., Liu, X., Pu, Y., & He, C. (2013). Olfactory ensheathing cells: the primary innate immunocytes in the olfactory pathway to engulf apoptotic olfactory nerve debris. *Glia*, *61*(4), 490-503. https://doi.org/10.1002/glia.22450

Tabakow, P., Raisman, G., Fortuna, W., Czyz, M., Huber, J., Li, D., Szewczyk, P., Okurowski, S., Miedzybrodzki, R., Czapiga, B., Salomon, B., Halon, A., Li, Y., Lipiec, J., Kulczyk, A., & Jarmundowicz, W. (2014). Functional regeneration of supraspinal connections in a patient with transected spinal cord following transplantation of bulbar olfactory ensheathing cells with peripheral nerve bridging. *Cell Transplant*, *23*(12), 1631-1655. https://doi.org/10.3727/096368914X685131

Takeoka, A., Jindrich, D. L., Munoz-Quiles, C., Zhong, H., van den Brand, R., Pham, D. L., Ziegler, M. D., Ramon-Cueto, A., Roy, R. R., Edgerton, V. R., & Phelps, P. E. (2011). Axon regeneration can facilitate or suppress hindlimb function after olfactory ensheathing glia transplantation. *J Neurosci*, *31*(11), 4298-4310. https://doi.org/10.1523/JNEUROSCI.4967-10.2011

Tepe, B., Hill, M. C., Pekarek, B. T., Hunt, P. J., Martin, T. J., Martin, J. F., & Arenkiel, B. R. (2018). Single-cell RNA-Seq of mouse olfactory bulb reveals cellular heterogeneity and activity-dependent molecular census of adult-born neurons. *Cell Rep*, *25*(10), 2689-2703 e2683. https://doi.org/10.1016/j.celrep.2018.11.034

Thornton, M. A., Mehta, M. D., Morad, T. T., Ingraham, K. L., Khankan, R. R., Griffis, K. G., Yeung, A. K., Zhong, H., Roy, R. R., Edgerton, V. R., & Phelps, P. E. (2018). Evidence of axon connectivity across a spinal cord transection in rats treated with epidural stimulation and motor training combined with olfactory ensheathing cell transplantation. *Exp Neurol*, *309*, 119-133. https://doi.org/10.1016/j.expneurol.2018.07.015

Trupp, M., Ryden, M., Jornvall, H., Funakoshi, H., Timmusk, T., Arenas, E., & Ibanez, C. F. (1995). Peripheral expression and biological activities of GDNF, a new neurotrophic factor for avian and mammalian peripheral neurons. *J Cell Biol*, *130*(1), 137-148. https://doi.org/10.1083/jcb.130.1.137

Ubink, R., Calza, L., & Hokfelt, T. (2003). 'Neuro'-peptides in glia: focus on NPY and galanin. *Trends Neurosci*, *26*(11), 604-609. https://doi.org/10.1016/j.tins.2003.09.003

Vincent, A. J., Choi-Lundberg, D. L., Harris, J. A., West, A. K., & Chuah, M. I. (2007). Bacteria and PAMPs activate nuclear factor kappaB and Gro production in a subset of olfactory ensheathing cells and astrocytes but not in Schwann cells. *Glia*, *55*(9), 905-916. https://doi.org/10.1002/glia.20512

Vincent, A. J., West, A. K., & Chuah, M. I. (2005). Morphological and functional plasticity of olfactory ensheathing cells. *J Neurocytol*, *34*(1-2), 65-80. https://doi.org/10.1007/s11068-005-5048-6

Wanner, I. B., Anderson, M. A., Song, B., Levine, J., Fernandez, A., Gray-Thompson, Z., Ao, Y., & Sofroniew, M. V. (2013). Glial scar borders are formed by newly proliferated, elongated astrocytes that interact to corral inflammatory and fibrotic cells via STAT3-dependent mechanisms after spinal cord injury. *J Neurosci*, *33*(31), 12870-12886. https://doi.org/10.1523/JNEUROSCI.2121-13.2013

Watzlawick, R., Rind, J., Sena, E. S., Brommer, B., Zhang, T., Kopp, M. A., Dirnagi, U., Macleod, M. M., Howells, D. Q.,Schwab, J. M. (2016) Olfactory ensheathing cell transplantation in experimental spinal cord injury: Effect size and reporting bias of 62 experimental treatments:A systematic review and meta-analysis. *PLOS Biol*, 14(5): e1002468. https://doi.org/10.1371/journal.pbio.1002468

Williams, S. K., Franklin, R. J., & Barnett, S. C. (2004). Response of olfactory ensheathing cells to the degeneration and regeneration of the peripheral olfactory system and the involvement of the neuregulins. *J Comp Neurol*, *470*(1), 50-62. https://doi.org/10.1002/cne.11045

Windus, L. C., Claxton, C., Allen, C. L., Key, B., & St John, J. A. (2007). Motile membrane protrusions regulate cell-cell adhesion and migration of olfactory ensheathing glia. *Glia*, *55*(16), 1708-1719. https://doi.org/10.1002/glia.20586

Witheford, M., Westendorf, K., & Roskams, A. J. (2013). Olfactory ensheathing cells promote corticospinal axonal outgrowth by a L1 CAM-dependent mechanism. *Glia*, *61*(11), 1873-1889. https://doi.org/10.1002/glia.22564

Woodhall, E., West, A. K., & Chuah, M. I. (2001). Cultured olfactory ensheathing cells express nerve growth factor, brain-derived neurotrophic factor, glia cell line-derived neurotrophic factor and their receptors. *Brain Res Mol Brain Res*, *88*(1-2), 203-213. https://doi.org/10.1016/s0169-328x(01)00044-4

Yates, A. D., Achuthan, P., Akanni, W., Allen, J., Allen, J., Alvarez-Jarreta, J., Amode, M. R., Armean, I. M., Azov, A. G., Bennett, R., Bhai, J., Billis, K., Boddu, S., Marugan, J. C., Cummins, C., Davidson, C., Dodiya, K., Fatima, R., Gall, A., . . . Flicek, P. (2020). Ensembl 2020. *Nucleic Acids Res*, *48*(D1), D682-D688. https://doi.org/10.1093/nar/gkz966

You, S., Petrov, T., Chung, P. H., & Gordon, T. (1997). The expression of the low affinity nerve growth factor receptor in long-term denervated Schwann cells. *Glia*, *20*(2), 87-100. https://doi.org/10.1002/(sici)1098-1136(199706)20:2

Figure legends

Figure 1. Transplanted GFP-OECs in the center of the lesion core associate with numerous axons. Sagittal sections show rostral and caudal glial scar borders of the injury site which are identified with glial fibrillary acidic protein (GFAP, blue). The GFAP-negative lesion core contains GFP-OECs (green) and is marked with asterisks. Arrowheads mark axons crossing into the lesion core. **(a-f)** Serotonergic axons (5-HT, red) are found in the rostral spinal cord stump and associate with OECs (green) in the lesion core. Single channels for GFAP **(c)**, OECs **(d)**, 5-HT **(e),** and a combination of 5-HT and OECs **(f)**. **(g-l)** Nearby injury site section from the same rat **(a)**. Numerous neurofilament-positive axons (white) are associated with the OECs (green) in the lesion core. Single channels for GFAP **(i)**, OECs **(j)**, neurofilament **(k),** and a combination of neurofilament and OECs **(l)**. Bridge formation across the injury site was observed in 2 of 8 OEC-transplanted and 0 of 11 fibroblast- or media-transplanted, spinal cord transected rats. Combined with the 1/5 OEC-transplanted rats with axons crossing the injury and 0/5 fibroblast controls in our previous study (Thornton, 2018), we observed bridges in 3/13 OEC-transplanted rats vs 0/16 controls (p=0.042, two-sample proportion test). Scale bars: a, g = 500 µm; b, h = 100 µm. Reprinted from: Dixie, KL, 2019, *UCLA*. ProQuest ID: Dixie_ucla_0031D_18445.

Figure 2. scRNA-seq results show distinct clusters of OECs and leftover cell samples. **(a)** Cells in tSNE plot colored by sample source, with cells from leftover samples in pink and cells from immunopurified OECs in cyan. **(b)** Clustering analysis revealed a total of 7 distinct cell clusters, each indicated with a different color. **(c)** A heatmap showing expression patterns of top marker genes of the 8 individual cell clusters. **(d)** Cell clusters showed distinct expression patterns for known cell type markers for fibroblasts, microglia, and OECs. Clusters 0, 1, and 5 had high expression of fibroblast markers and are labeled as fibroblast in the Y-axis; clusters 4,

6, and 7 showed high expression of microglia markers and are labeled as microglia; clusters 2, 3, and 7 showed high expression of OEC markers and are labeled as OEC. Known marker genes for different cell types are on the X-axis. Feature plots and violin plots for select marker genes are in Suppl. Figure 1. **(e)** Based on known cell type markers, cell clusters in tSNE plot were labeled with the corresponding cell types. **(f)** The expression of cell-type specific marker genes is depicted in a dot plot. **(g)** Genes that distinguish purified OECs vs OECs in leftover cultures are shown. The top 3 genes were higher in purified OECs, whereas the bottom 3 genes were higher in 'leftover' cultures.

Figure 3. Well-established OEC markers are revealed by scRNA-seq and immunofluorescence.

OEC cultures were replated from extra cells prepared for scRNA-seq. Immunolabeled OECs are marked with arrows and all cell nuclei are stained with Hoechst (blue nuclei). tSNE maps of the gene expression in the 5 clusters are shown next to the protein expression in a-l. **(a, b)** Cultured OECs express Ngfr^{p75} protein and *Ngfr*^{p75} gene expression. **(c, d)** Blbp and Sox10 immunoreactive OECs with *Fabp7* gene expression. **(e, f)** S100β-labeled OECs together with *S100β* expression. **(g, h)** L1cam and Sox 10 labeling next to *L1cam* expression. **(i, j)** Ncam1 protein and gene expression**. (k, l)** N-Cadherin and Sox10 markers with *Cdh2* expression. **(m-p)** scRNA-seq data for *Sox10, Cntf, Itga7*, and *Mpz* (references in text). Scale bars: a, c, e, g, i, k = 50 µm.

Figure 4. OEC subclusters, marker genes, and enriched pathways.

(a) Clustering analysis of OECs revealed five separate clusters (0-4). **(b)** Heatmap depicts the expression patterns of known marker genes of glial cell types (x-axis) versus microglia, all OECs and OEC subclusters (y-axis). OEC subclusters express select markers of other glial cell types. **(c)** Heatmap depicts the top five marker genes (y-axis) for each OEC subcluster (x-axis). **(d)** Pathways associated with marker genes of different OEC clusters are shown. The dashed line indicates the false discovery rate (FDR) <0.05 in the pathway analysis. **(e)** Dot plot showing that cluster 3 has higher potential lysosomal function based on lysosome pathway genes than the other clusters. **(f)** Both cluster 3 and 4 express select genes involved in positive regulation of cell migration. **(g)** Trajectory analysis reveals two trajectories, one including subclusters 2, 0, and 4, and another involving subclusters 2, 0, 1, and 3. **(h)** NicheNet ligand-receptor network plot demonstrates intracellular communication between OEC subtypes. Hexagons represent subclusters 0 to 4 and circles indicate ligands secreted from subclusters. Edges (arrows) point to clusters where receptors of the ligands are expressed. Different colors represent different OEC subclusters.

Figure 5. Confirmation of *Ccn2/Ctgf* (Connective tissue growth factor) in cultured OECs and following OEC implantation after spinal cord injury.

(a, b) The scRNA-seq plots of the 9th (*Ccn2/Ctgf)* and 4th (*Ccn3*/*Nov*) highest-ranked marker genes are strongly expressed in subcluster 0. **(c, c1, c2)** The well-known matricellular protein Connective tissue growth factor (Ctgf) identifies OECs in cell cultures (red, c, c2), and Sox10 nuclear expression (white nuclei, c, c2) confirms they are neural crest-derived cells. **(d, d1, d2)** A sagittal section from a rat that received a complete spinal cord transection followed by Green Fluorescent Protein (GFP)-OEC implantation was fixed 2 weeks postinjury. Glial fibrotic acidic protein (d, Gfap, blue) marks the edges of the borders of the glial scar. GFP-OECs (green) that

express Ctgf (red) in the injury site are outlined by the box in d. High expression of Ctgf is detected by GFP-OECs that bridge part of the injury site in d1. The single channel of Ctgf is shown in d2. Scale bars: c-c2 = 50 µm, d-d2 = 250 µm.

Figure 6. Subcluster 2 is characterized by cell cycle and proliferative markers.

(a-f) These scRNA-seq plots show high expression of cell proliferation markers in cluster 2, supporting their function as OEC progenitor cells. Only *Stmn1* (e, Stathmin, a microtubule destabilizing protein) is broadly expressed across all five clusters. **(g-g2, h-h2)** Most cultured OECs are spindle-shaped and have high $Ngfr^{p75}$ expression (red, white arrows). Of the OEC progenitors that express Ki67, 76% ± 8 of them display low levels of $Ngfr^{p75}$ immunoreactivity and a "flat" morphology (g2, h2; green nuclei, arrowheads). The remainder of Ki67-expressing OECs express high levels of $Ngfr^{p75}$ and are fusiform in shape (24% ± 8%, n=4 cultures, Student-t test, p= 0.023). Hoechst marks all nuclei (g1, h1, blue nuclei, arrowheads). Scale bars: g, h = 50 µm.

Figure 7. Spatial confirmation of the defined OECs subclusters within the olfactory nerve layer.

The protein expression of a number of top 20 genes from this scRNA-seq study of purified OEC cultures is verified in olfactory bulb sections. In all images, the olfactory nerve layer (ONL, layer I) is at the bottom of the image, the glomeruli (GL, layer II) next, and the remainder of the olfactory bulb toward the top. Suppl. figure 2 illustrates the corresponding tSNE plots for each gene in Figure 7. **(a-c)** The top gene in the largest cluster, Peripheral myelin protein 22, is highly expressed throughout the ONL. Gliomedin, the third-ranked gene in cluster 0, is detected as small discrete dot-like structures overlaying the ONL (b, box enlarged in c). **(d-f)** OECs in

cluster 1 are immunolabeled by antibodies against the axonal growth factor Atf3 (d) and the intermediate filament Nestin (f). High levels of Gap43 in the ONL (e) are due to expression by OECs and axons of immature olfactory sensory neurons. **(g-i)** Strong immunoreactivity of Stathmin-1 in the ONL reflects labeled axons from immature olfactory sensory neurons and OECs. Ube2c, a G2/M cell cycle regulator, is expressed in a small number of cells in the ONL, whereas Mki67-labeled cells are widespread. **(j-l)** The immune function of this cluster is confirmed by antibodies against Apoe (j), Anxa3 (k), and Aif1/Iba1, markers expressed by microglia and macrophages. Scale bars: a, b, d-l = 50 µm; c, insets in j-l = 25 µm.

Figure 8. Reelin-signaling pathway marker genes in OEC clusters and Reelin immunoreactivity in embryonic olfactory system.

(a-f) These six tSNE plots show OEC gene expression levels associated with Reelin signaling. *Reln* is highly expressed in most OEC clusters (a), *Disabled-1* (*Dab1*, b), and *Apolipoprotein E receptor 2* (*Apoer2*, c) show little expression, and *Very-low-density lipoprotein receptor* has moderate expression (*Vldlr*, d). The serine protease tissue Plasminogen Activator (e, *tPA*) is highly expressed in all OEC subsets and cleaves secreted Reelin only at its C-terminus. ADAMTS-4 cleaves both the N- and C-terminals of Reelin, and is expressed at low levels by OECs (f). **(g-g2)** Sagittal section of the olfactory epithelium (OE) and olfactory bulb from an E16.5 *Reln*$^{+/+}$ mouse immunolabeled for Blbp (g, g1; red) and Reelin (g, g2; green). Boxed area in g is enlarged in g1 and g2. Axons of olfactory sensory neurons (arrows) are surrounded by peripheral OECs that express both Blbp (g1, arrowheads) and Reelin (g2, arrowheads). High Reln expression is obvious in olfactory bulb neurons (g, g1, green) but the olfactory nerve layer (ONL) only expresses Blbp (g, g2). **(h, h1)** No Reelin is detected in a sagittal section from a

Reln$^{-/-}$ mouse, yet Blbp expression in the ONL appears normal. Scale bars: g-h = 50 µm; g1, g2 = 50 µm.

Figure 9. Reelin is expressed and secreted by olfactory ensheathing cells.

(a-c) Rat OEC cultures were treated with Brefeldin-A to inhibit protein transport and subsequent secretion. Reelin immunoreactivity (red) in a primary culture was detected in GFP-labeled OECs (a, arrows), but not in another cell type (arrowhead). GFP-labeled OECs which were immunopurified with anti-Ngfr^{p75} also express Reelin (red; b, c). **(d)** Western blot confirms the expression of Reelin in rat Olfactory Nerve Layer I and II (ONL; lane 1 of western blot). *Reln*$^{+/+}$ and *Reln*$^{-/-}$ mouse olfactory bulbs were used as positive and negative controls, respectively (lanes: 2 and 3). Reelin synthesized by cultured OECs was found at low levels in whole cell lysates (WCL; lanes: 4, 6, and 8), compared to Reelin secreted by cultured OECs into tissue culture medium, termed OEC "conditioned medium" (CM; lanes: 5 and 7). GAPDH was the loading control for tissue homogenates (lanes 1-4, 6, 8). **(e)** All three Reelin isoforms (400, 300, and 150 kDa) were detected with a 4-15% gradient gel. *Reln*$^{+/+}$ and *Reln*$^{-/-}$ mouse cortices were used as controls (lanes: 1 and 2). Reelin was detected in the rat ONL (lane 3) and in three rat OEC-CM samples (lanes: 4, 5, and 6). GAPDH was the loading control for tissue homogenates (lanes: 1-3). **(f)** Quantitation of multiple isoforms of Reelin from 4-15% gradient gels. Positive and negative controls are *Reln*$^{+/+}$ and *Reln*$^{-/-}$ mouse cortices. Both rat tissue from the ONL (n=3) and CM (n=9) contain significantly more 400 and 300 kDa Reelin than the *Reln*$^{-/-}$ mice. Bars represent the standard deviation of the mean. One-sided Mann-Whitney U test was used to test that protein expression levels in the other groups are greater than those in the *Reln*$^{-/-}$ group, indicative of significant expression of *Reln* in the test groups. *$p < 0.05$. Scale bars: a-c = 40 µm.

Supplemental Figures

Figure S1. Marker genes were expressed specifically in different areas associated with Figure 2.

(a-c) Marker genes characteristic of OECs **(a)**, Microglia **(b)**, and fibroblasts **(c)** are shown in their tSNE plots (top) and violin plots (bottom).

Figure S2. The tSNE plots corresponding to the OEC subclusters illustrated in Figure 7.

(a-b) Cluster 0 tSNE plots show that *Pmp22* is expressed in all 5 clusters with *Gldn* concentrated in clusters 0, 2, and 4. **(d-f)** For cluster 1, tSNE plots illustrate a wide distribution of *Atf3* and *Nes*, whereas *GAP43* is found primarily in cluster 1. **(g-i)** The cell cycle and proliferative markers, *Ube2c* and *Mki67*, appear limited to cluster 2, but *Stmn1* is detected in all clusters but most heavily concentrated in cluster 2. **(j-l)** Cluster 3 tSNE plots show high expression of *Apoe*, *Anxa3*, and *Aif1*, but *Apoe* is also expressed in other clusters.

Figure S3. Violin plots for quality control

(a) Before quality control measurement. **(b)** After quality control measurement. nFeature_RNA indicates gene counts; nCount RNA indicates unique molecular identifier (UMI) counts; percent.mt indicates mitochondria content. Samples (x-axis) are labeled by concatenation of batch (1 or 2), type (OEC or leftover), and sample ID.

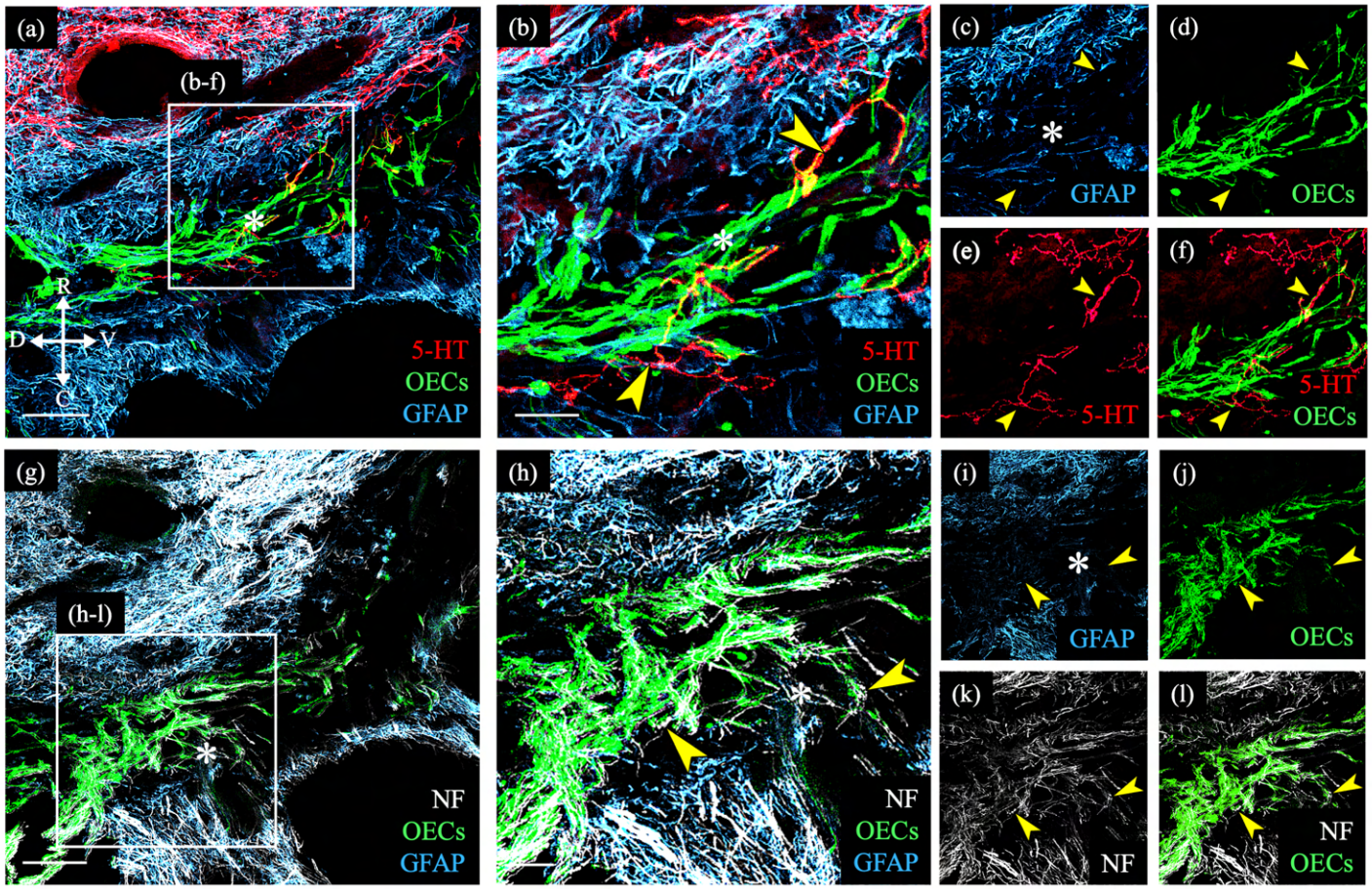
(a)
(b-f)
R
D
V
C
5-HT
OECs
GFAP
(b)
5-HT
OECs
GFAP
(c)
GFAP
(d)
OECs
(e)
5-HT
(f)
5-HT
OECs
(g)
(h-l)
NF
OECs
GFAP
(h)
NF
OECs
GFAP
(i)
GFAP
(j)
OECs
(k)
NF
(l)
NF
OECs

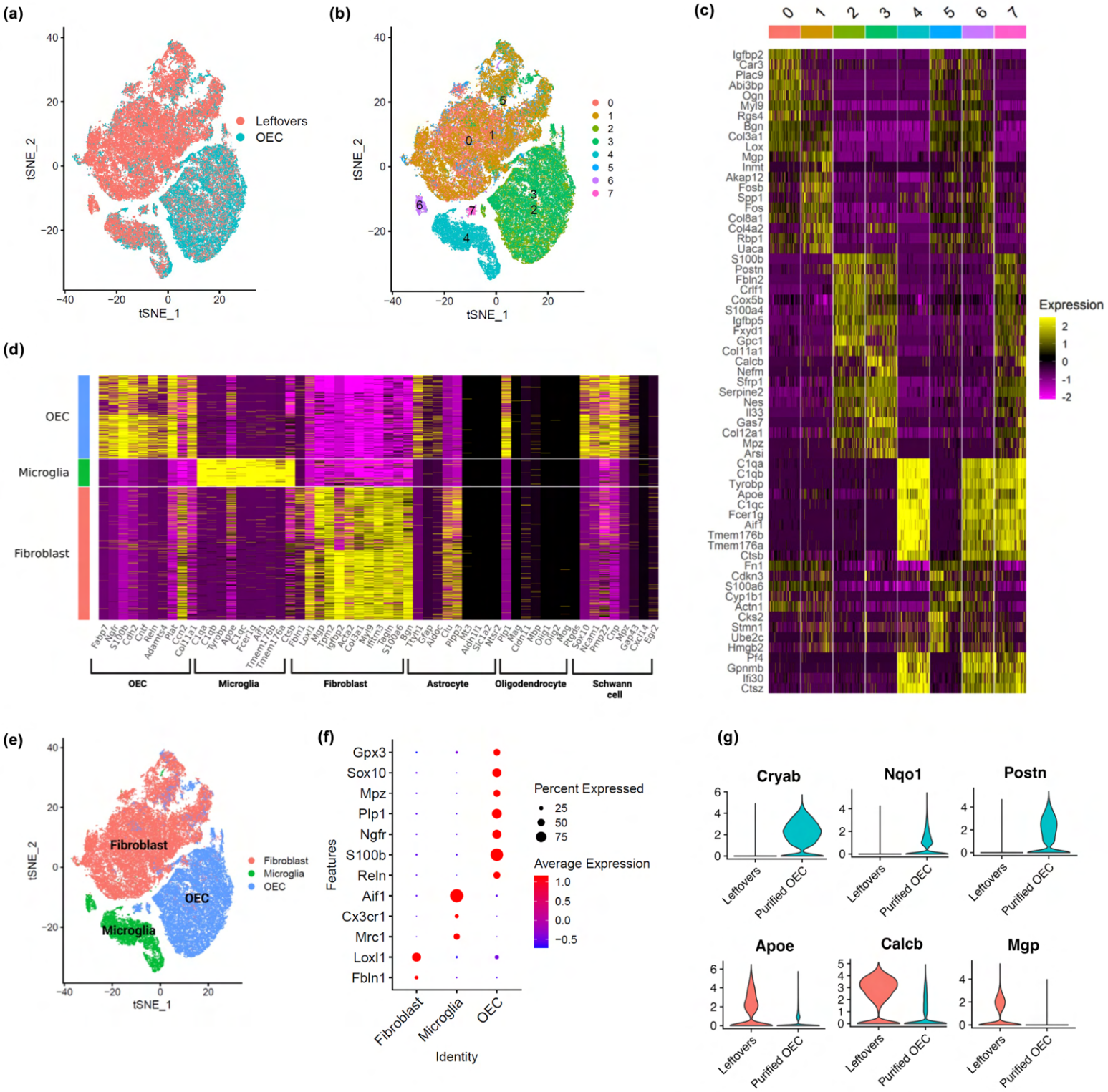
(a)
Leftovers
OEC
tSNE_1
tSNE_2
(b)
0
1
2
3
4
5
6
7
(c)
Expression
(d)
OEC
Microglia
Fibroblast
Astrocyte
Oligodendrocyte
Schwann cell
(e)
Fibroblast
Microglia
OEC
(f)
Percent Expressed
Average Expression
Features
Identity
(g)
Cryab
Nqo1
Postn
Apoe
Calcb
Mgp
Leftovers
Purified OEC

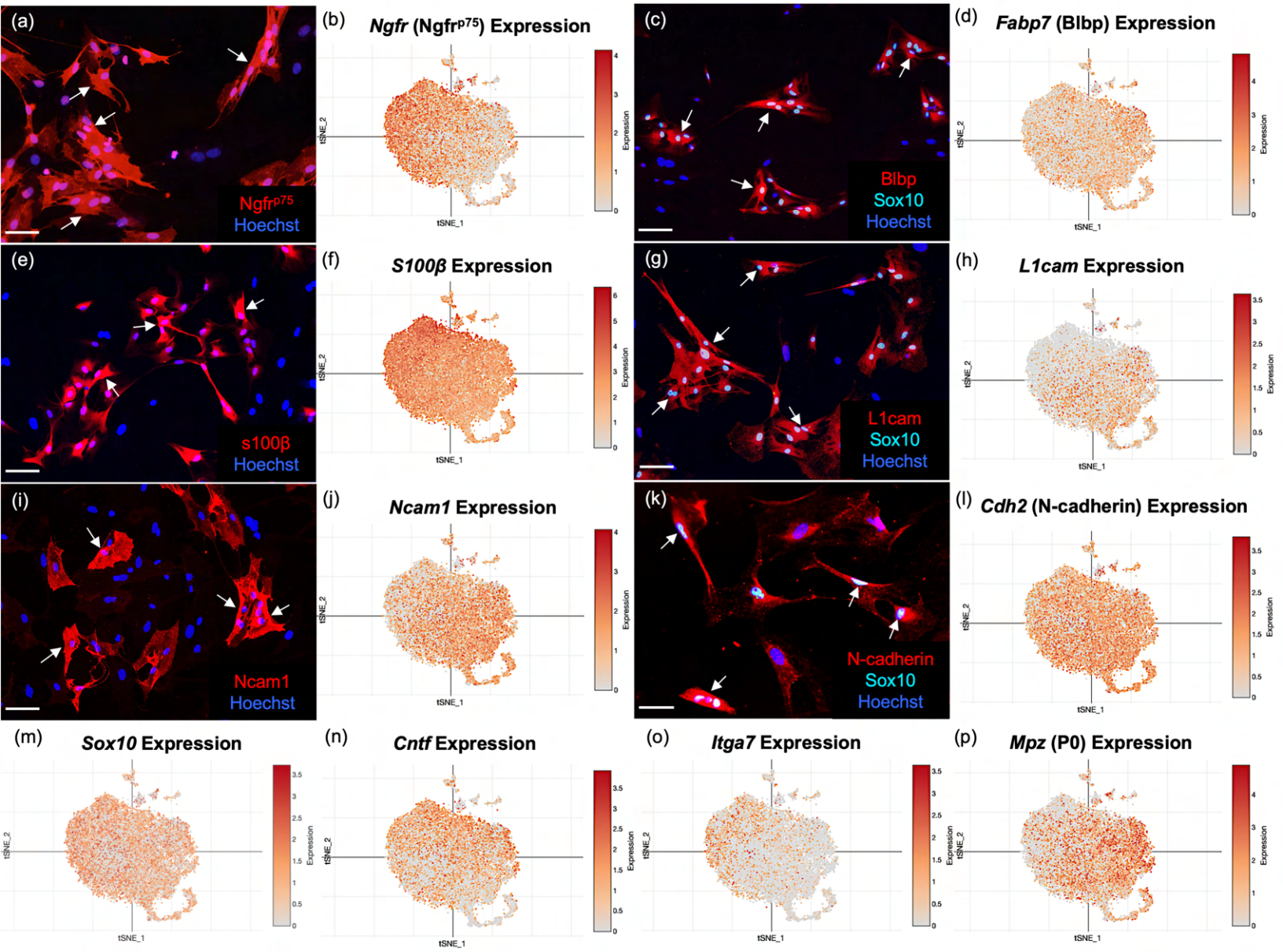

(m) *Sox10* Expression

(n) *Cntf* Expression

(o) *Itga7* Expression

(p) *Mpz* (P0) Expression

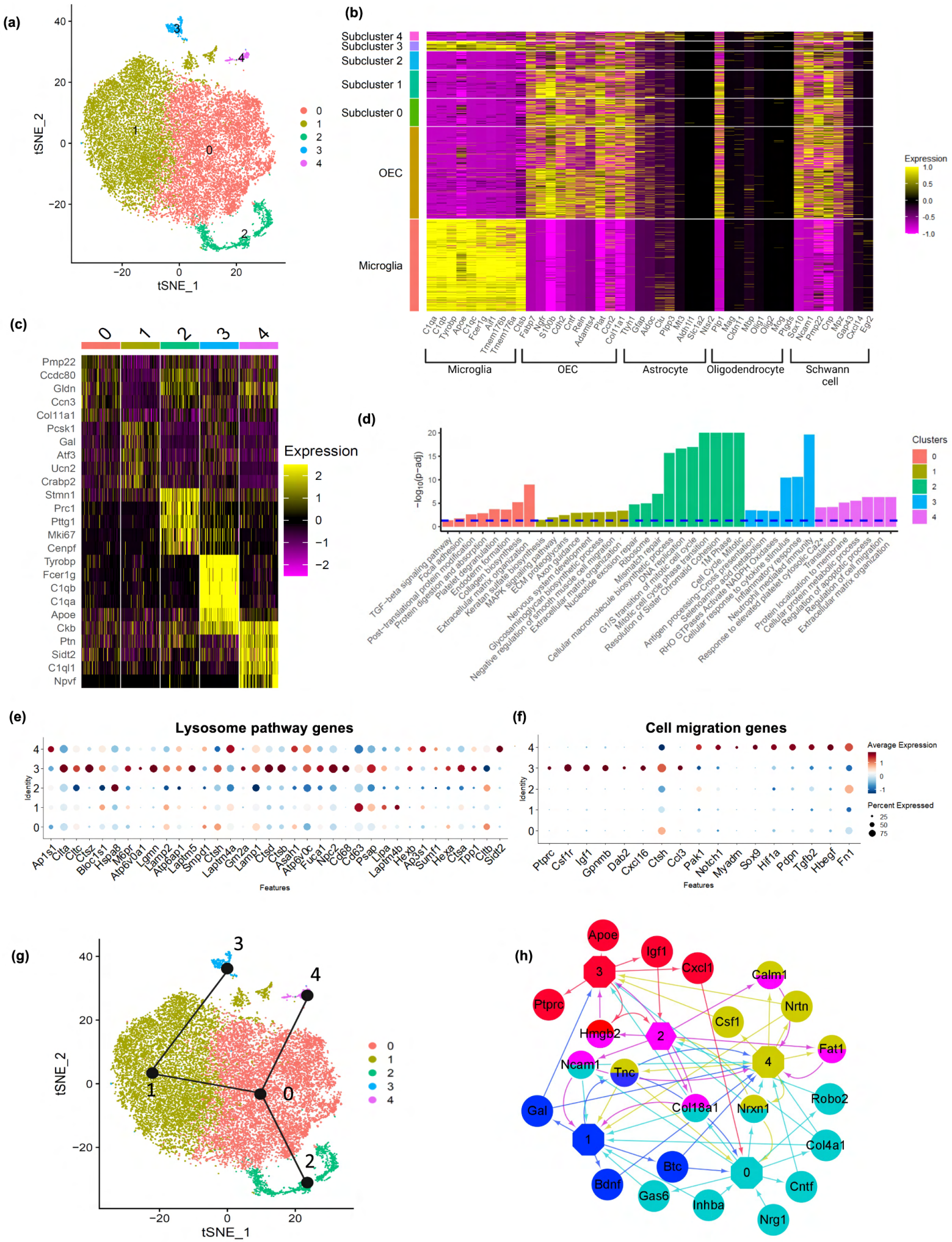
(a)
tSNE_2
tSNE_1
0
1
2
3
4
(b)
Subcluster 4
Subcluster 3
Subcluster 2
Subcluster 1
Subcluster 0
OEC
Microglia
Expression
Microglia
OEC
Astrocyte
Oligodendrocyte
Schwann cell
(c)
Pmp22
Ccdc80
Gldn
Ccn3
Col11a1
Pcsk1
Gal
Atf3
Ucn2
Crabp2
Stmn1
Prc1
Pttg1
Mki67
Cenpf
Tyrobp
Fcer1g
C1qb
C1qa
Apoe
Ckb
Ptn
Sidt2
C1ql1
Npvf
Expression
(d)
−log10(p−adj)
Clusters
TGF−beta signaling pathway
Post−translational protein modification
Focal adhesion
Protein digestion and absorption
Platelet degranulation
Endoderm formation
Collagen biosynthesis
Extracellular matrix organization
Keratan sulfate biosynthesis
MAPK signaling pathway
ECM proteoglycans
Nervous system development
Axon guidance
Glycosaminoglycan biosynthesis
Negative regulation of smooth muscle cell migration
Extracellular matrix organization
Nucleotide excision repair
Ribosome
Mismatch repair
Cellular macromolecule biosynthesis
DNA replication
G1/S transition of mitotic cell cycle
Mitotic cell cycle phase transition
Resolution of Sister Chromatid Cohesion
M Phase
Cell Cycle, Mitotic
Antigen processing−Cross presentation
Selenoamino acid metabolism
RHO GTPases Activate NADPH Oxidases
Cellular response to cytokine stimulus
Inflammatory response
Neutrophil mediated immunity
Response to elevated platelet cytosolic Ca2+
Protein localization to membrane
Cellular protein metabolic process
Regulation of apoptotic process
Regulation of cell migration
Extracellular matrix organization
(e)
Lysosome pathway genes
Identity
Features
(f)
Cell migration genes
Identity
Features
Average Expression
Percent Expressed
(g)
tSNE_2
tSNE_1
(h)
Apoe
Igf1
Cxcl1
Calm1
Ptprc
Nrtn
Csf1
Hmgb2
Fat1
Ncam1
Tnc
Robo2
Gal
Col18a1
Nrxn1
Col4a1
Btc
Bdnf
Gas6
Inhba
Cntf
Nrg1

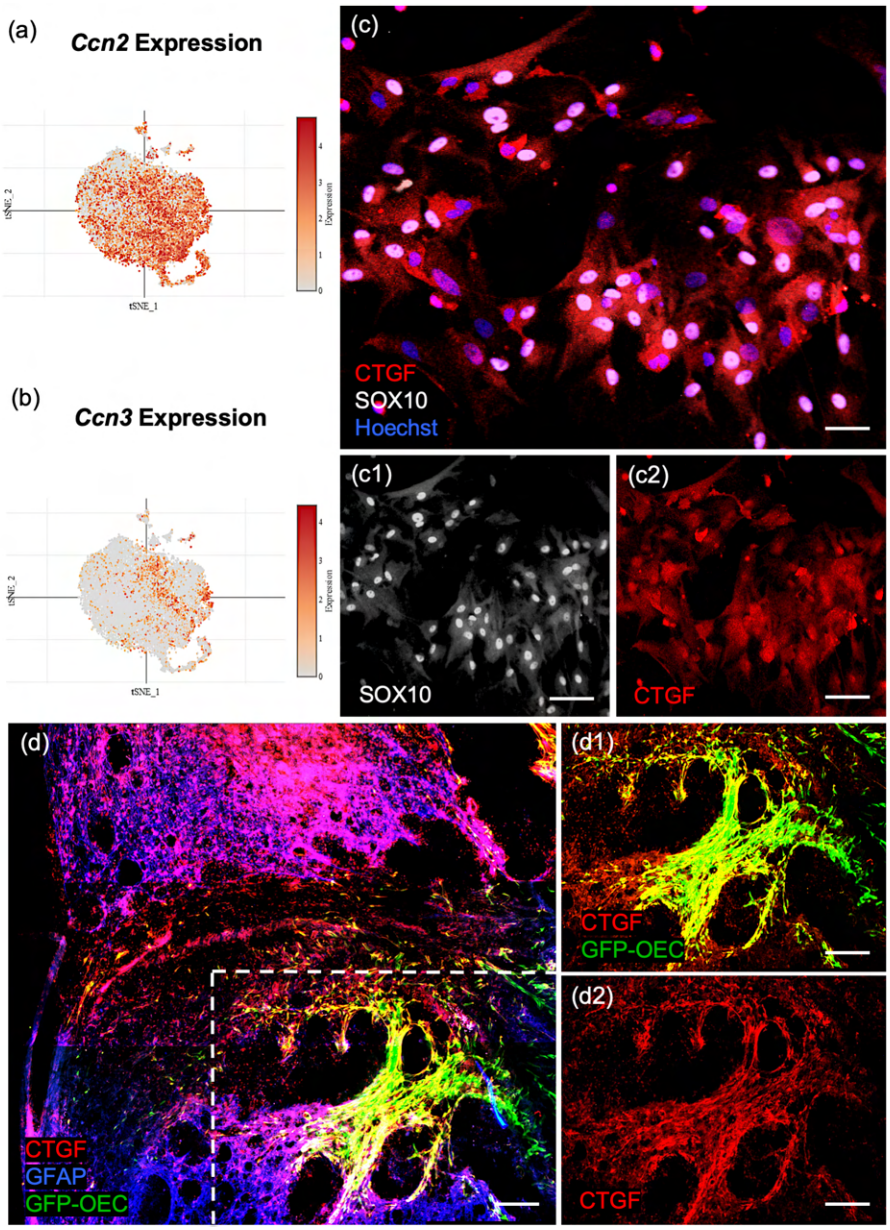
(a)
Ccn2 Expression
tSNE_2
tSNE_1
Expression
(b)
Ccn3 Expression
tSNE_2
tSNE_1
Expression
(c)
CTGF
SOX10
Hoechst
(c1)
SOX10
(c2)
CTGF
(d)
CTGF
GFAP
GFP-OEC
(d1)
CTGF
GFP-OEC
(d2)
CTGF

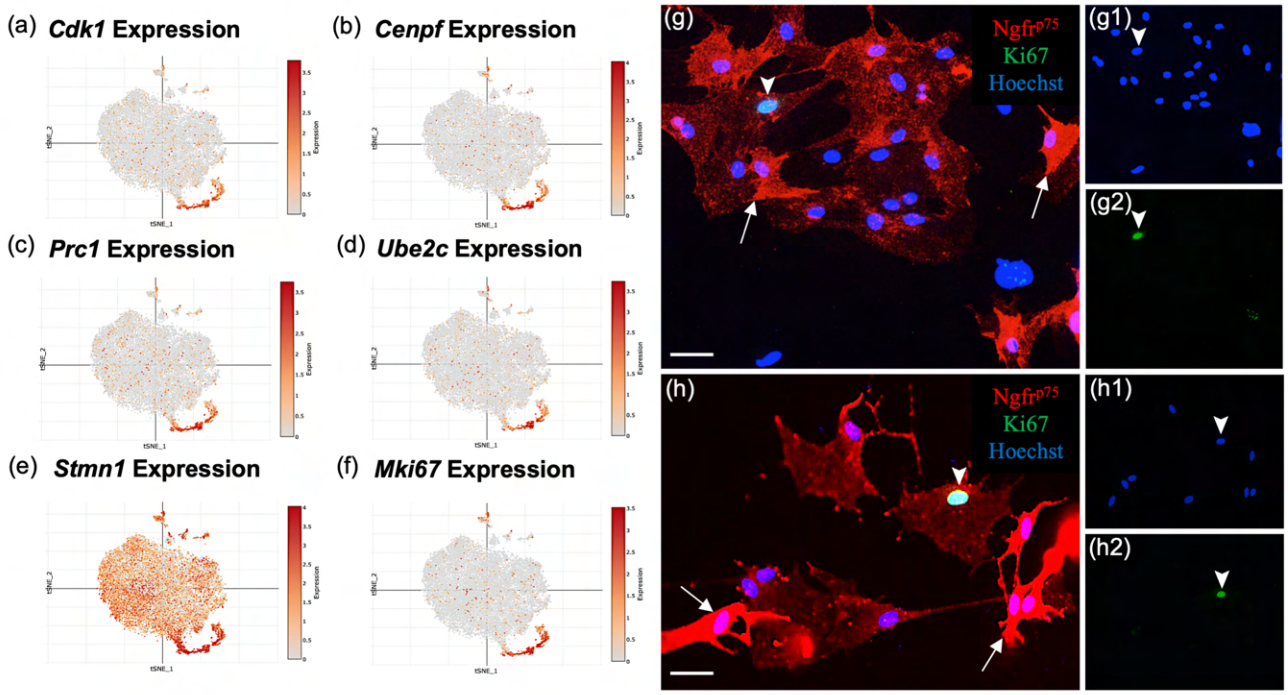
(a) Cdk1 Expression
(b) Cenpf Expression
(c) Prc1 Expression
(d) Ube2c Expression
(e) Stmn1 Expression
(f) Mki67 Expression
tSNE_1
tSNE_2
Expression
(g)
Ngfrp75
Ki67
Hoechst
(g1)
(g2)
(h)
Ngfrp75
Ki67
Hoechst
(h1)
(h2)

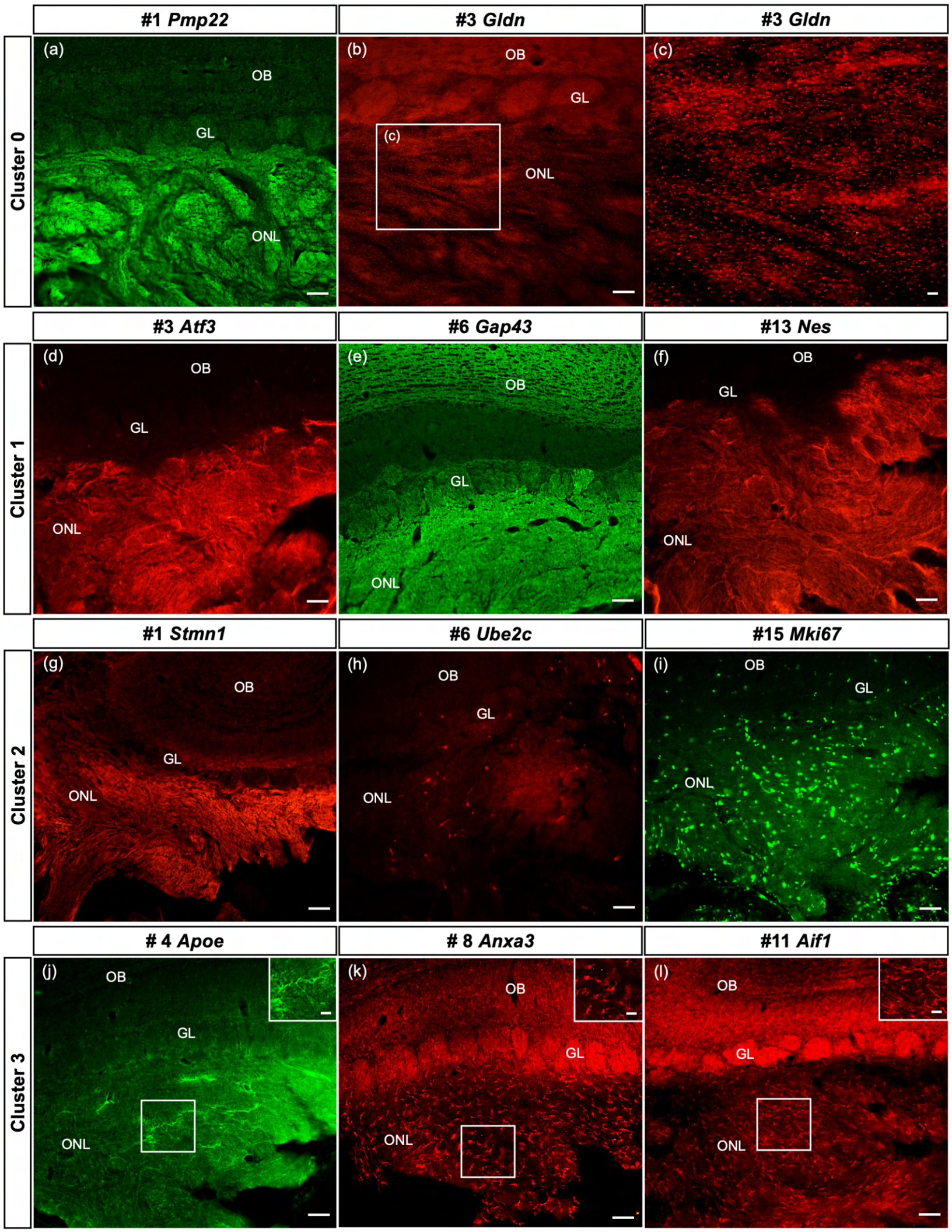
#1 Pmp22
#3 Gldn
#3 Gldn
Cluster 0
(a)
OB
GL
ONL
(b)
OB
GL
(c)
ONL
(c)
#3 Atf3
#6 Gap43
#13 Nes
Cluster 1
(d)
OB
GL
ONL
(e)
OB
GL
ONL
(f)
OB
GL
ONL
#1 Stmn1
#6 Ube2c
#15 Mki67
Cluster 2
(g)
OB
GL
ONL
(h)
OB
GL
ONL
(i)
OB
GL
ONL
4 Apoe
8 Anxa3
#11 Aif1
Cluster 3
(j)
OB
GL
ONL
(k)
OB
GL
ONL
(l)
OB
GL
ONL

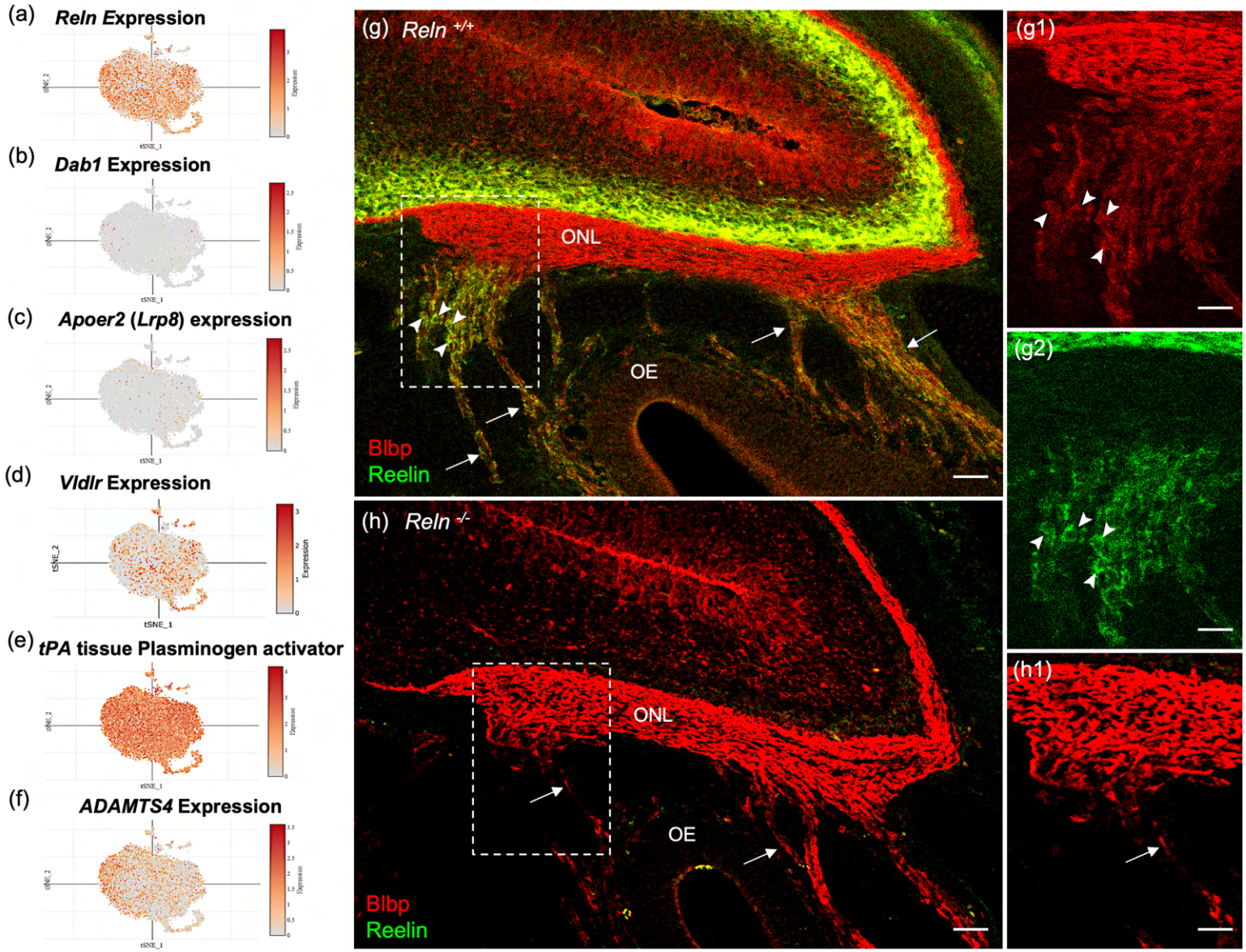
(a) Reln Expression
(b) Dab1 Expression
(c) Apoer2 (Lrp8) expression
(d) Vldlr Expression
(e) tPA tissue Plasminogen activator
(f) ADAMTS4 Expression
tSNE_1
tSNE_2
Expression
(g) Reln +/+
ONL
OE
Blbp
Reelin
(g1)
(g2)
(h) Reln -/-
ONL
OE
Blbp
Reelin
(h1)

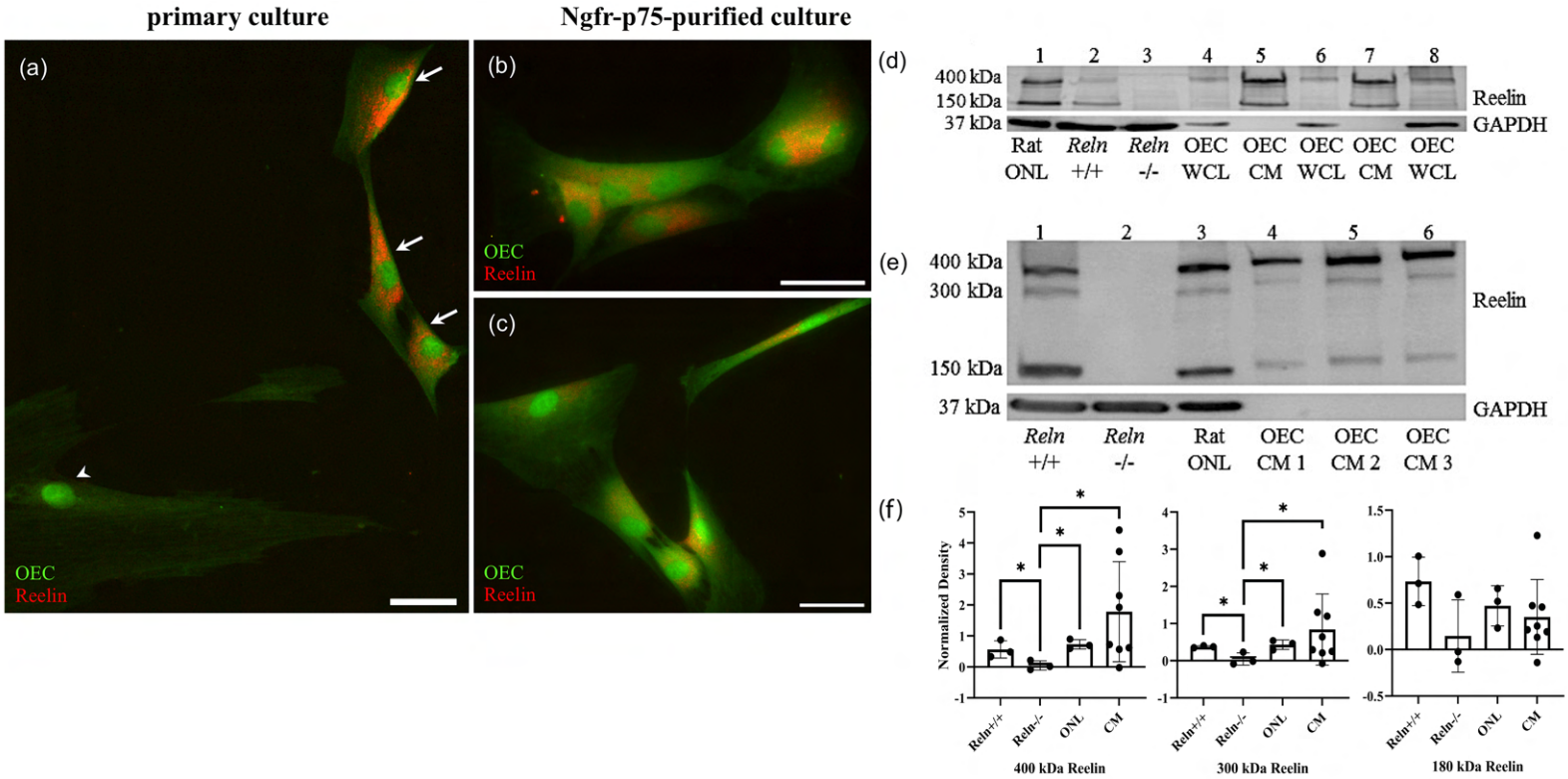
primary culture
Ngfr-p75-purified culture
(a)
OEC
Reelin
(b)
OEC
Reelin
(c)
OEC
Reelin
(d)
1 2 3 4 5 6 7 8
400 kDa
150 kDa
37 kDa
Reelin
GAPDH
Rat ONL
Reln +/+
Reln -/-
OEC WCL
OEC CM
OEC WCL
OEC CM
OEC WCL
(e)
1 2 3 4 5 6
400 kDa
300 kDa
150 kDa
37 kDa
Reelin
GAPDH
Reln +/+
Reln -/-
Rat ONL
OEC CM 1
OEC CM 2
OEC CM 3
(f)
Normalized Density
Reln+/+
Reln-/-
ONL
CM
400 kDa Reelin
300 kDa Reelin
180 kDa Reelin